ABSTRACT

RUTHRAUFF, ALICIA ANN. The Effects of Pulsatile Fatigue on *in situ* Radiofrequency Fenestrated Endovascular Stent Grafts Deployed Inside a Semi-Realistic Model of an Aneurysmal Abdominal Aorta. (Under the direction of Dr. Martin W. King).

An abdominal aortic aneurysm or AAA is a localized dilation of the aorta in the abdominal region whose cause is unknown [1]. It can be found in 1.3% of men 45-54 years old, and 12.5% of men 75-84 years old [2]. With a 90% chance of mortality after rupture, this disease is serious [2].

The two surgical techniques (open repair and endovascular repair) currently used to repair the aneurysms are limited when the aneurysm is located close to or above the renal arteries that lead to the kidneys. The length of landing zone required for the less-invasive procedure, endovascular aneurysm repair (EVAR), would require that the stent be placed above the renal arteries, which would interrupt the blood flow to the kidneys [7]. Therefore techniques for fenestrating the stent material to allow continued blood flow through the renal arteries are currently being studied.

One technique uses a radiofrequency puncture wire to fenestrate the device *in situ* after the endograft has been deployed, then subsequently using angioplasty balloons to increase the size of the fenestration so a stent can be inserted through the fenestration and into the renal artery, anchoring them together would allow for off-the-shelf devices to be used without the increased waiting period required for pre-fenestrated devices [9-12, 14-15].

A previous study using this technique [15] looked at the performance of the flat fabric when subjected to those fenestration conditions. The current study focused on the performance

of the entire device deployed inside of a semi-realistic model of the aorta in order to observe changes in physical and mechanical characteristics after being pulsatile fatigued for the equivalent of one year *in vivo.* Six specimens were used in this study, three Cook Zenith Flex® and three Medtronic Endurant®. In order to additionally test whether or not the addition of a cutting balloon during the procedure would assist in keeping the fenestration open and not occluding the renal stent, one of each kind of device was fenestrated with the aid of a cutting balloon.

The devices were fatigued then explanted from the models and macroscopically and microscopically analyzed. The fenestration areas were measured and the fabric counts taken around the immediate fenestration area. The probe bursting resistance was also measured. The macro and microscopic analyses showed evidence of melted fibers and frayed fibers on all fenestrations. The fraying was seen more on the devices fenestrated with a cutting balloon, and overall more fraying was seen on the Endurant devices compared to the Zenith devices. Small areas where the fabric had unraveled could also be seen on both devices that used a cutting-balloon. The probe bursting resistance was highest for the control fabric without fenestration or fatigue, then next highest for the samples that didn't use a cutting balloon, then lowest for the samples that did use a cutting balloon.

The overall results were favorable for this technique. The damage that occurred to the fibers in terms of fraying and melting did not occur beyond the fenestration area. The low bursting strength for the samples that used a cutting balloon can most likely be attributed to the larger fenestration size. More long-term research should be performed with a larger sample size to verify these results.

The Effects of Pulsatile Fatigue on *in situ* Radiofrequency Fenestrated Endovascular Stent Grafts Deployed Inside a Semi-Realistic Model of an Aneurysmal Abdominal Aorta

by
Alicia Ann Ruthrauff

A thesis submitted to the Graduate Faculty of
North Carolina State University
in partial fulfillment of the
requirements for the degree of
Master of Science

Textile Engineering

Raleigh, North Carolina

2013

APPROVED BY:

_____	_____
Dr. Martin W. King Committee Chair	Dr. Marian McCord
_____	_____
Dr. Julie Willoughby	Dr. Leonard Tse

DEDICATION

To my Mom and Dad, for all of their love and support!

BIOGRAPHY

Alicia Ruthrauff was born and raised in Howell, New Jersey in 1988. She attended Philadelphia University where she obtained a Bachelor's degree in Engineering with a concentration Textile Engineering. She was accepted into the Master's degree program for Textile Engineering at North Carolina State University in 2010. Here she worked under the direction Dr. Martin King on her Master's thesis. She expects to graduate in August 2013 and plans to find employment in the medical textile industry.

ACKNOWLEDGMENTS

I would like to acknowledge and thank Dr. Martin King; without his guidance, kindness, and infinite wisdom and patience, I could never have completed this project. I wish to thank him for always being available and willing to help me at any time, with any problem. I would also like to thank Dr. Marian McCord and Dr. Julie Willoughby for being a part of my committee and providing valuable feedback.

In addition, I would like to thank the numerous other people I worked with. I would like to thank Leslie Eadie for her work, which provided the starting point for my own. I would like to thank Dr. Leonard Tse for his dedication to this project, and for helping me understand and appreciate the clinical importance of it. I would also like to thank Dr. Tse and Dr. KT Tan for performing the fenestrations and obtaining not only the devices I needed but also procuring the many other pieces of equipment needed to perform the fenestrations. I would like to thank Dr. J.P. Urbanski and Baylis for providing the radiofrequency puncture device and for travelling to Toronto for the 'surgery' in order to make sure it performed properly. Thank you to Dr. Gilles Soulez for sharing his phantom concept and for working with myself and Boris Chayer to modify it to fit on our fatigue tester. Additional thanks to Boris for manufacturing the modified phantoms. Thank you to the very patient Matt Thompson from Bose Enduratec, as well as the rest of the support staff, for helping me whenever the fatigue tester had a problem. Thank you to Dr. Mark Farber for all of his feedback and suggestions during the planning of this project, as well as for obtaining and deploying the Cook devices.

I would additionally like to thank my research group and all of my friends for their support, and for listening to me and providing advice. Last but not least, thank you to my parents. I could not have completed this project without your infinite love and support.

TABLE OF CONTENTS

LIST OF FIGURES

LIST OF TABLES

CHAPTER 1: INTRODUCTION

An abdominal aortic aneurysm is a localized swelling or dilation of the aorta in the abdominal region. It develops slowly over years and often does not display any symptoms in the patient until it ruptures [1]. The mortality rate after rupture is as high as 90% [2]. There are three treatment options available for a patient who presents with an abdominal aortic aneurysm. If the aneurysm is smaller than 5.0-5.5 cm the physician will usually choose to carefully monitor it for any growth rather than have the patient undergo an expensive and risky surgery [3]. If the aneurysm is larger, it has a greater risk of rupture so the physician will choose to intervene via one of two surgical routes [4].

Traditional open surgery requires the opening of the patient's abdominal cavity in order to expose the aneurysm, which is then cut open so a vascular graft can be inserted and sewn into place [5]. The alternative to this surgery is a minimally invasive endovascular surgery also known as EVAR (Endovascular Aneurysm Repair) surgery. It was popularized in 1991 by Dr. Juan Parodi [6] and involves the deployment of an endovascular stent graft via the femoral arteries.

Most AAAs are infrarenal, initiating below the renal arteries. However, many patients experience pararenal aneurysms, which include juxtarenal aneurysms that originate at the renal arteries, and suprarenal aneurysms, which originate above the renal arteries. Use of EVAR is limited in these aneurysms because the landing zone for the proximal end, or the proximal neck, has to be a certain length in order to obtain proper fixation for the device [7]. In pararenal aneurysms, the proximal neck may be located above the renal arteries, and accordingly the placement of the device would cover the renal arteries, occluding them.

In these situations, where the patient cannot undergo either open surgery (due to not being eligible for risk reasons) or EVAR surgery, the device must be fenestrated at the renal arteries to allow blood to continue to flow to the kidneys. There is currently only one FDA approved device that meets this criteria. The Cook Zenith Fenestrated® Endovascular Stent Graft System is a custom made device based off of the successful traditional EVAR device, the Cook Zenith Flex®. CT scans of the patient's anatomy are used to make custom fenestrations to fit the patient's unique aortic morphology [8]. The amount of time it takes to manufacture each unique device can be up to 6-12 weeks, a long time for a patient with a critical condition. There is also no guarantee that the patient's anatomy will not change during this time, nor does this device allow for the repair of ruptured aneurysms due to that amount of time required [9-12].

There are currently studies going on for other methods of fenestration or branching that can be applied to off the shelf devices. These include mini-cuffs being sewn to fenestrations [9], hybrid/extra-anatomic bypass, chimneys/snorkels, off the shelf fenestrated devices, custom branches being sewn to fenestrations [13, 23], and RF puncture *in situ* fenestration [14-15]. All of these are currently being studied for their efficacy.

1.1 Problem Statement

All of the studies on *in situ* fenestration to date focus on a case to case basis only, and in one case was performed on canines, not humans [14]. Most of the research also focuses on the clinical aspects of the new technique rather than the effect on the graft, especially on the fabric of the graft which makes up the majority of the device.

Without an idea of the long term behavior of the fenestrated fabric *in vivo*, there are chances that endoleaks and subsequent ruptures could occur. A small tear caused by the fenestration might propagate due to fatigue. The previous study on this particular type of *in situ* fenestration aimed to show the effects of RF puncture on flat fabric representative of the fabric on the device [15]. This study was illuminating and very novel. However, the behavior of the stent graft as a whole and after undergoing realistic pulsatile pressures and different types of fenestrations is still not fully understood.

1.2 Goals and Objectives

The goal of this study is to determine and demonstrate the effects of *in situ* antegrade fenestration and the effect of two different types of subsequent ballooning on the integrity of endovascular stent grafts. By cycling them for the equivalent of one year *in vivo* on a pulsatile fatigue tester, the structural integrity of both the graft fabric and the stent components can be determined using *in vitro* evaluation methods. The concern is that the fenestrations will weaken the surrounding fabric, and that over time that fabric will continue to weaken due to positive and pulsatile blood pressure, and become a potential site for an endoleak. To test this theory two different models of stent grafts will be deployed into a realistic model of an aorta with a short necked abdominal aortic aneurysm. They will then be fenestrated, ballooned, and stented to mimic what would occur in surgery at the time of implantation. RF puncture will be performed followed by two different kinds of balloon angioplasty, one using a standard angioplasty balloon and the other using a cutting balloon. As there will only be one stent graft of each brand for each type of fenestration, this will be a

demonstration study rather than an experimental study relying on statistical analysis. The stent grafts will be mounted in a pulsatile fatigue tester for 40 million cycles, which is the equivalent of 1 year of in vivo exposure. The following properties of the grafts will be measured before and after fatiguing, in order to answer the following questions:

1. Are the warp and weft counts affected differently by use of a cutting balloon, and do they change after pulsatile fatigue?
2. Is the force required to burst the fabric with a probe different when a cutting balloon is used, and how does pulsatile fatigue affect the probe bursting resistance?
3. Are there any macroscopic or microscopic differences in the structure around the fenestration after fatigue between the normal RF puncture and the RF puncture with a cutting balloon? The two stent grafts that were selected for use in this study (Medtronic's Endurant and Cook's Zenith) were chosen based on their popularity of use by surgeons for patients with short-necked abdominal aortic aneurysms.

CHAPTER 2: REVIEW OF LITERATURE

2.1 Introduction to AAA

An abdominal aortic aneurysm is a weakening of the arterial walls that leads to a localized dilation in the abdominal region of the aorta, as seen in Figure 1. To be considered truly aneurysmal the dilation must be at least a 50% increase in diameter. Eventually these aneurysms can rupture, with a mortality rate of 90% once ruptured [2].

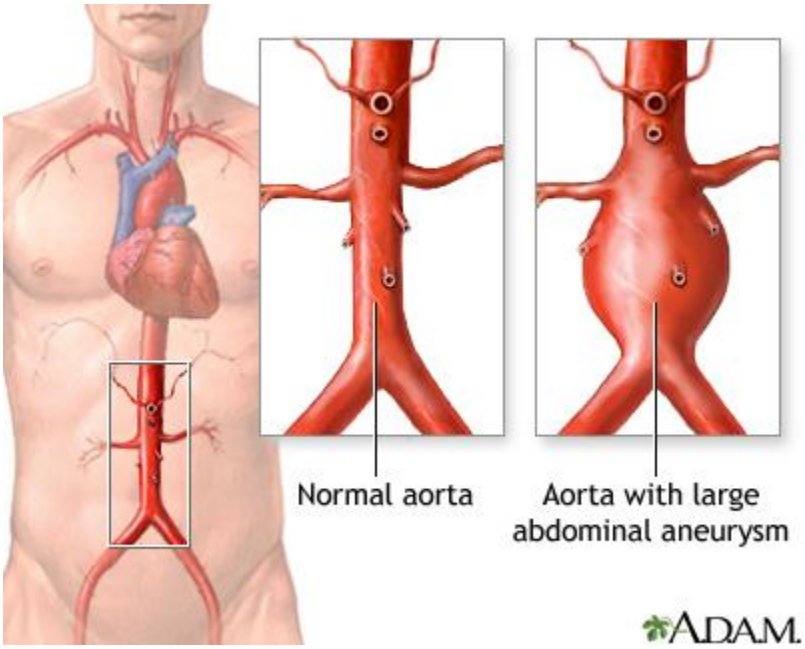

Figure 1: An illustration comparing a normal aorta with an aneurysmal aorta 16].

There are several types of aneurysms. The most common are aneurysms associated with atherosclerosis (known as atherosclerotic aneurysms), but whether atherosclerosis is a cause, risk factor, or response is still unknown, due to poor understanding of the mechanism

behind the formation of an aortic aneurysm. In the Tromsø study performed by Johnsen et al, 6446 men and women had an ultrasound performed on their right carotid artery, femoral artery, and abdominal aorta to find a correlation between atherosclerosis and abdominal aortic aneurysms. While there was a correlation between aneurysms larger than 27 mm in diameter and increased incidence of atherosclerosis and coronary heart disease, in aneurysms smaller than 27 mm in diameter the amount of carotid plaque forming the atherosclerosis did not relate to the diameter of the aneurysm. Due to this the study did not conclude that atherosclerosis is the cause of abdominal aortic aneurysms, but rather suggested that it develops in parallel with AAA or as a result of AAA [17].

Atherosclerotic aneurysms account for nearly 90% to 95% of all abdominal aortic aneurysms. The other 5-10% are known as inflammatory abdominal aortic aneurysms (IAAAs) [18-19]. They differ from atherosclerotic aneurysms in several ways. IAAAs generally affect younger patients and are more likely to be symptomatic than typical AAAs, presenting with back or abdominal pain and an elevated erythrocyte sedimentation rate. While diagnosed in the same way as atherosclerotic aneurysms, they present differently in that they show fibrosis of the adjacent retroperitoneum, a significant thickening of the aortic wall, and signs that adjacent structures stick to the aneurysm wall (See Figure 2). There are several theories on how these develop. All of the theories agree that the inflammation is a result of an immune response in the adventitia of the aorta, but what causes this immune response is not agreed upon. One theory suggests that the antigen is a lipid or a product of lipid oxidation, such as is found in atherosclerotic aneurysms. Since inflammatory cells are present in all patients with AAA, and atherosclerosis is largely associated with AAA, it is a strong possibility that the

presence of lipid cells in the aorta causes vascular inflammation. Others theorize that IAAAs are caused by an infectious disease, most notably *Chlamydia pneumonia* and cytomegalovirus [19].

Yet others have linked IAAAs to autoimmune diseases due to large amounts of antinuclear antibodies and antineutrophil cytoplasmic antibodies seen in the patients. A study found that 19% of 31 patients with an IAAA co-presented with an associated autoimmune disease. However, not all of the patients presented with the same autoimmune disease, and with the number of patients being small to begin with, the link between autoimmune diseases and IAAA is fairly weak [19-20].

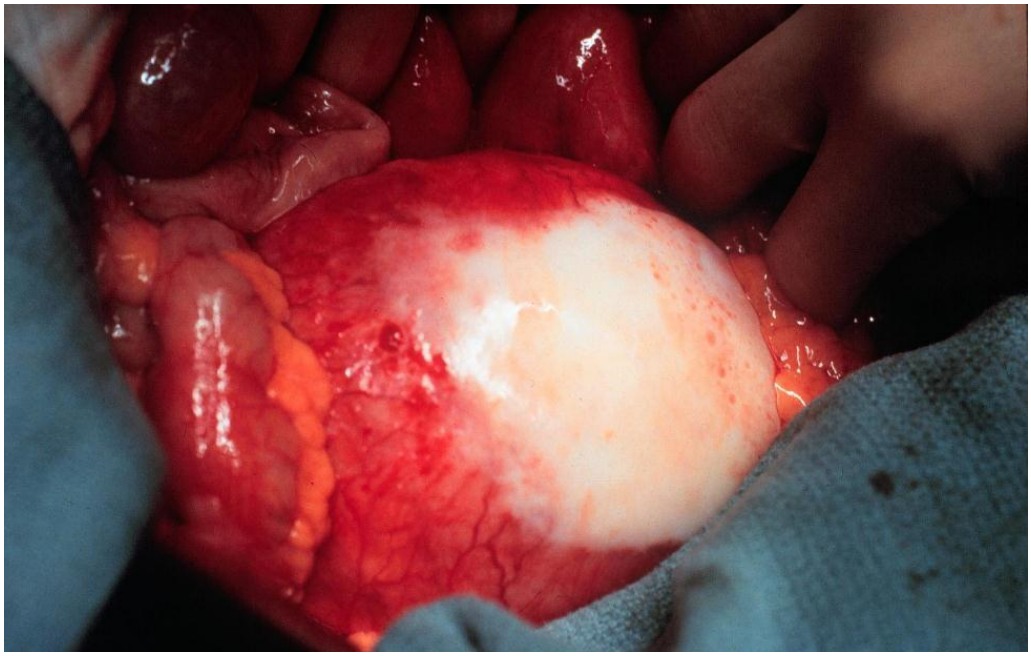

Figure 2: Inflammatory Aneurysm with retroperitoneal fibrosis and adhesion of the duodenum and fibrosis [21].

Abdominal aortic aneurysms present in three different ways in terms of shape. Fusiform aneurysms, the most typical, are mostly symmetrical bulges that occur around the entire circumference of the aorta. Saccular aneurysms only appear on part of the circumference and appear like a balloon attached to the aorta. They are often caused by a trauma to the aorta, including a severe aortic ulcer [22]. A false aneurysm or pseudoaneurysm is a cavity that forms in between the inner and outer layers of the aorta due to a tear in the inner layer that allows arterial blood to flow in between the layers. It can form into a saccular aneurysm [23]. An aortic dissection is similar in that in only affects some of the aortic layers. It usually occurs in the thoracic region of the aorta, but can occur in the abdominal region. Figure 3 shows these three types of aneurysms, and Figure 4 shows an aortic dissection [24].

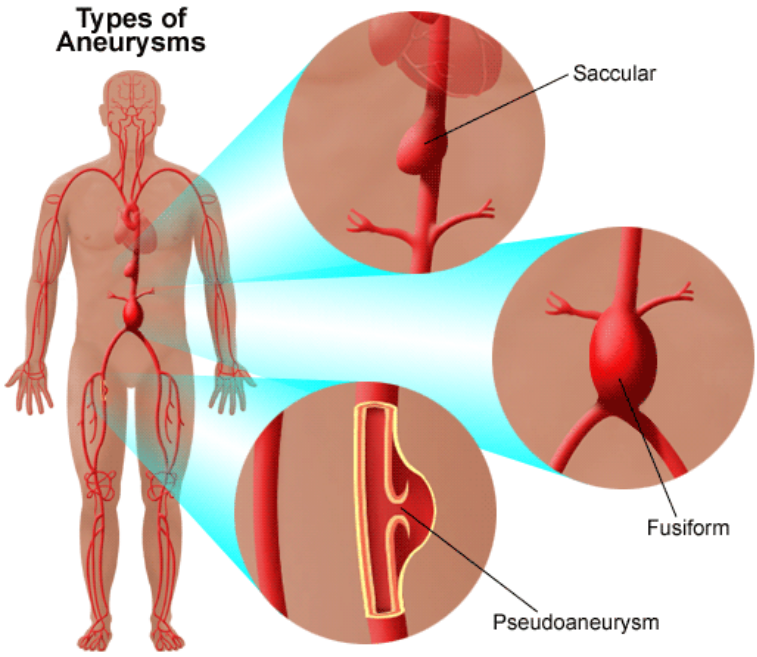

Figure 3: Different aneurysmal shapes [24].

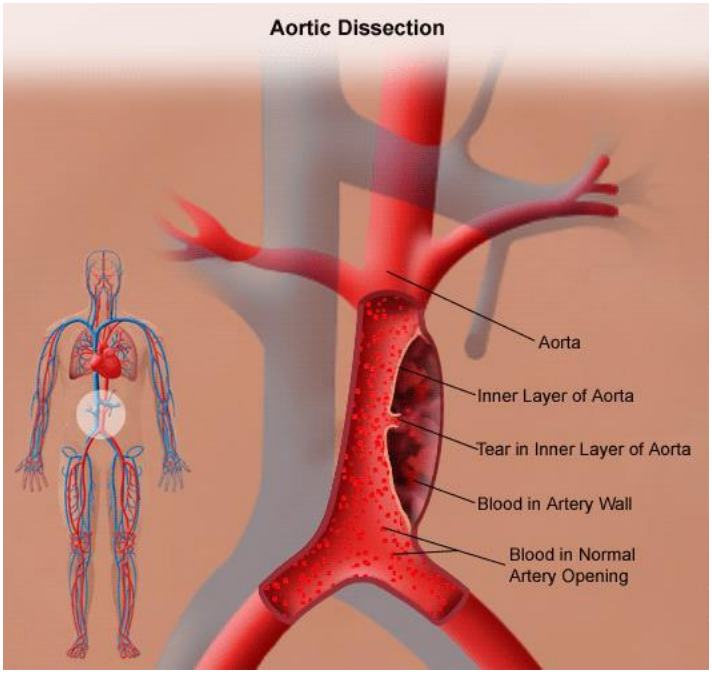

Figure 4: Detailed view of Pseudoaneurysm/Aortic Dissection [24]

2.2 Risk factors

There are several risk factors for aortic aneurysms, those being a history of smoking, a family history of aortic aneurysms, high blood pressure, high cholesterol, atherosclerosis, inheritable conditions like Marfan's syndrome, infection, and trauma. Most abdominal aortic aneurysms are associated with atherosclerosis [2]. Atherosclerosis is a thickening of the arterial walls due to collection of fat, causing the artery to expand to accommodate the extra material [24] though as stated earlier this is not universally agreed upon. As the aneurysm grows, the risk of rupture also rises. With a diameter over 5 cm, the risk of a rupture is around 20%. At 6 cm, the risk rises to 40%, and over 7 cm the risk is at 50% [2]. The average annual expansion rates also change with size. Aneurysms less than 4 cm in diameter expand approximately 1-4 mm a year, aneurysms 4-6 cm in diameter expand approximately 4-5 mm a year, and aneurysms larger than 6 cm in diameter expand 7-8 mm a year [4]. A comparison of risk of rupture for various risk factors can be seen in Table 1.

Table 1: Risk of Abdominal Aortic Aneurysm Rupture for Various Risk Factors [4]

	Low Risk	**Average Risk**	**High Risk**
Diameter	< 5 cm	5-6 cm	>6 cm
Expansion	< 0.3 cm/y	0.3-0.6 cm/y	>0.6 cm/y
Smoking/COPD	None, mild	Moderate	Severe/steroids
Family history	No relatives	One relative	Numerous relatives
Hypertension	Normal blood pressure	Controlled	Poorly controlled
Shape	Fusiform	Saccular	Very eccentric
Wall stress	Low (35 N/cm^2	Medium (40 N/cm^2	High (45 N/cm^2)
Sex	...	Male	Female

2.3 Statistics

Abdominal aortic aneurysms are most common in older Caucasian males. They can be found in 1.3% of men 45-54 years old, and 12.5% of men 75-84 years old [2]. Less than 1% of women aged 45-54 years and 5.2% of women aged 75-84 years have abdominal aortic aneurysms ranging between 2.9 and 4.9 cm in diameter. In the United States in 2009 there was a total of 2,437,163 deaths, 10,597 having been caused by aortic aneurysms or aortic dissections, meaning that they caused 0.43% of the total number of death [16]. In spite of the general decline in mortality over the years [2], the number of deaths in 2010 caused by aortic aneurysms was 13,238, with the any-mention mortality number of 18,800. Any-mention mortality means that comorbidities were present, and the actual cause of death was hard to identify. The total number of hospital discharges for aortic aneurysms was 57,000, meaning that the number of incidences of aortic aneurysms in 2010 was 75,800 [4].

Once a patient is diagnosed with an abdominal aortic aneurysm, there are three paths the doctor can suggest. If the aneurysm is small the risk of rupturing is small, so the doctor will likely decide to closely monitor it instead of performing surgery. A study by Watson et al showed that aneurysms smaller than 4 cm are relatively benign and that surgery does not provide a noticeable benefit to the patient [3]. If the aneurysm has a larger risk of rupture, there are two types of surgeries the doctor can choose to perform, open repair and endovascular repair.

2.4 Open Repair

In open repair a long cut is made into the patient's abdomen and the skin, muscle, and organs are gently pulled away until the aneurysm is exposed (See Figure 5). The aorta is then clamped above and below the aneurysm and the aneurysm is cut open. A vascular graft is sewn

into place, and the clamps are undone to make sure there are no leaks (See Figure 6). The aneurysm is then closed with sutures, and the stomach is stapled closed [5].

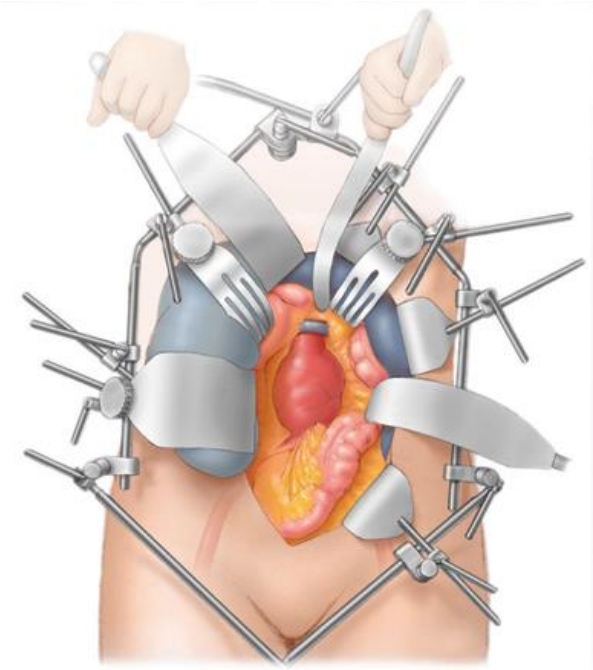

Figure 5: The first major step in open repair, opening the abdominal cavity to reveal the aneurysm [5].

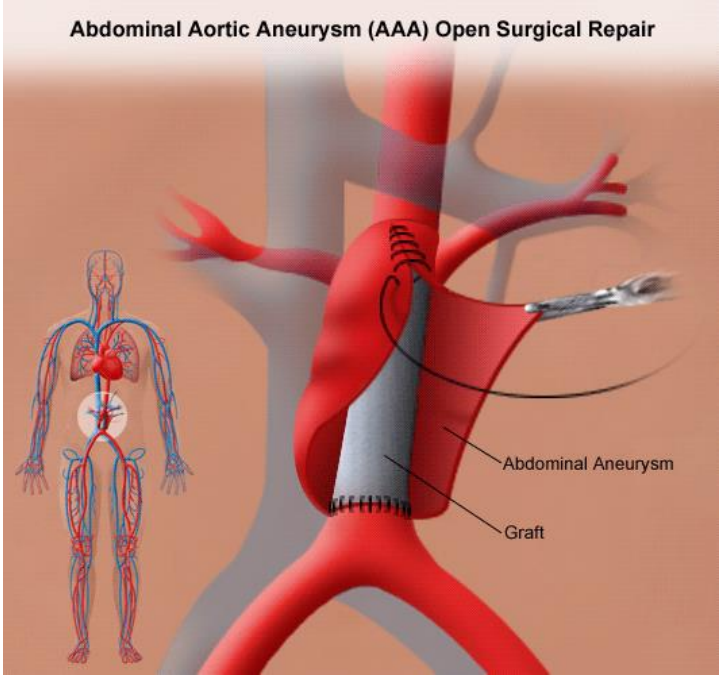

Figure 6: After the graft is sewn into place the aneurysm is sewn back around it [24].

2.5 Endovascular Repair

In endovascular repair, the aneurysm is bypassed using a totally percutaneous method (See Figure 7). An endovascular stent graft contained inside a catheter is inserted through the femoral artery in the patient's leg and guided up the iliac arch and into the aorta until it is properly positioned. The positioning is done using fluoroscopy to visualize the stent graft, which contains several radiopaque markers specifically for positioning. Depending on the instructions for use, a balloon catheter may or may not be inserted to ensure full expansion of the device. Extensions are then inserted into the openings at the bottom end of the stent graft and are ballooned open to secure them to each side of the iliac arch. The only incisions made

during this surgery are small ones made in the femoral arteries in the leg. The graft is held in place by the metal stents at the top (see Figure 8), which often have hooks attached to avoid long term migration [15].

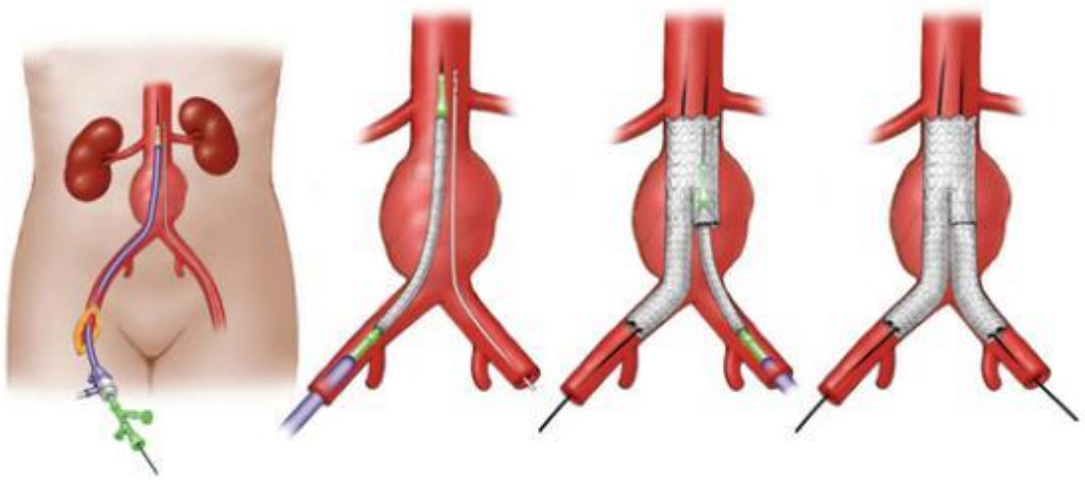

Figure 7: Standard endovascular *stent graft deployment for an infrarenal abdominal Aortic Aneurysm [5]*.

2.6 Open Repair versus EVAR

Several studies have been done comparing the effectiveness of open repair versus endovascular repair. A study by Peterson et al included 99 patients who had undergone open repair and 235 patients who had undergone endovascular repair and followed them for five years. No deaths were caused by aneurysm rupture for either method, and they found that the aneurysm-related survival was not significantly different between the methods. There was a significant difference in the number of major adverse events that occurred in each group. Major adverse events here refers to events that require hospitalization, both short and long term,

therapy, requires permanent adverse sequelae, or requires death [25]. The number of MAE in EVAR patients was significantly lower than in open repair patients at every time point.

Nedeau et al reviewed seventy four records of repaired ruptured infrarenal AAAs from May 2000 to September 2010 for perioperative mortality, midterm survival, acute limb ischemia, length of stay, respiratory failure, myocardial infarction, abdominal compartment syndrome, and secondary intervention. Rupture refers to a tear forming in the aortic wall leading to arterial blood leaking into the abdominal cavity. Nineteen of these ruptured aneurysms were repaired using EVAR and fifty-five by open repair. Perioperative mortality rates were 15.7% and 49% for EVAR and open repair, respectively. At one year 60% of the EVAR patients had survived versus 45% of open repair patients. Acute limb ischemia, myocardial infarction, and acute renal failure rates post-surgery were similar for both groups. Length of stay was on average shorter for EVAR patients (10 days) versus open repair (21 days). The percentage of patients requiring reintervention were similar for both groups. Overall the study recommends the use of EVAR for repair of ruptured aortic aneurysms on the basis of superior survival rates [27].

Paravastu et al compared open repair versus EVAR in inflammatory abdominal aortic aneurysms using 35 studies comprising of a total of 999 open repair patients and 21 studies with 121 EVAR patients. They found that thirty day mortality was 6% for open repair and 2% for EVAR, and one year mortality (all causes) rose to 14% for open repair and remained at 2% for EVAR. Periaortic inflammation regressed in 73% of open repair patients and 65% of EVAR patients, but inflammation progressed more in EVAR patients (4%) than in open repair patients (1%). Hydronephrosis, a post-operative problem associated with IAAAs, increased in 21% of

EVAR patients versus only 9% of open repair patients. The study was inconclusive as to whether open repair or endovascular repair is better overall. However, they did conclude that EVAR is associated with lower one year mortality, and that open repair is preferable for low-risk patients who already have hydronephrosis [28].

Overall it seems that EVAR is preferable in terms of long term mortality rates. However it must be noted that there are disputes over the consistency of long term mortality rates across studies. Saqib et al believe that many biases contribute to the general belief that EVAR for rAAA has superior long term survival rates, and conclude that it does not actually have any advantage over open repair at all. Their biases are as follows: non-randomized trials (i.e. poor patient selection), publication bias, and limited follow-up [29].

2.7 Problems

2.7.1 Endoleak

Endoleaks are a leakage of the aortic arterial blood flow into the aneurysmal sac after surgical intervention. When persistent, they can cause the aneurysm to rupture, leading to mortality. A categorization system proposed by Veith et al separates them into four different kinds of endoleaks (See Figure 8) [30]. Type I endoleaks are leaks that occur at the distal or proximal fixation sites. Type II endoleaks are caused by retrograde flow from small vessels covered by the stent graft back into the sac. Type III endoleaks are caused by defects in the stent-graft material, such as holes or tears. Improper seal between the main body and the extensions is also included under Type III. Type IV endoleaks are caused by the porosity of

the textile component. There is an additional classification called type V, used when there is no visible endoleak but the aneurysmal sac is still enlarging. The pressure causing it to enlarge in these cases is referred to as endotension. Type V are the most unusual and are only found in 2% to 5% of patients that have undergone EVAR surgery. In total, endoleaks occur in 15-52% of patients [31-32].

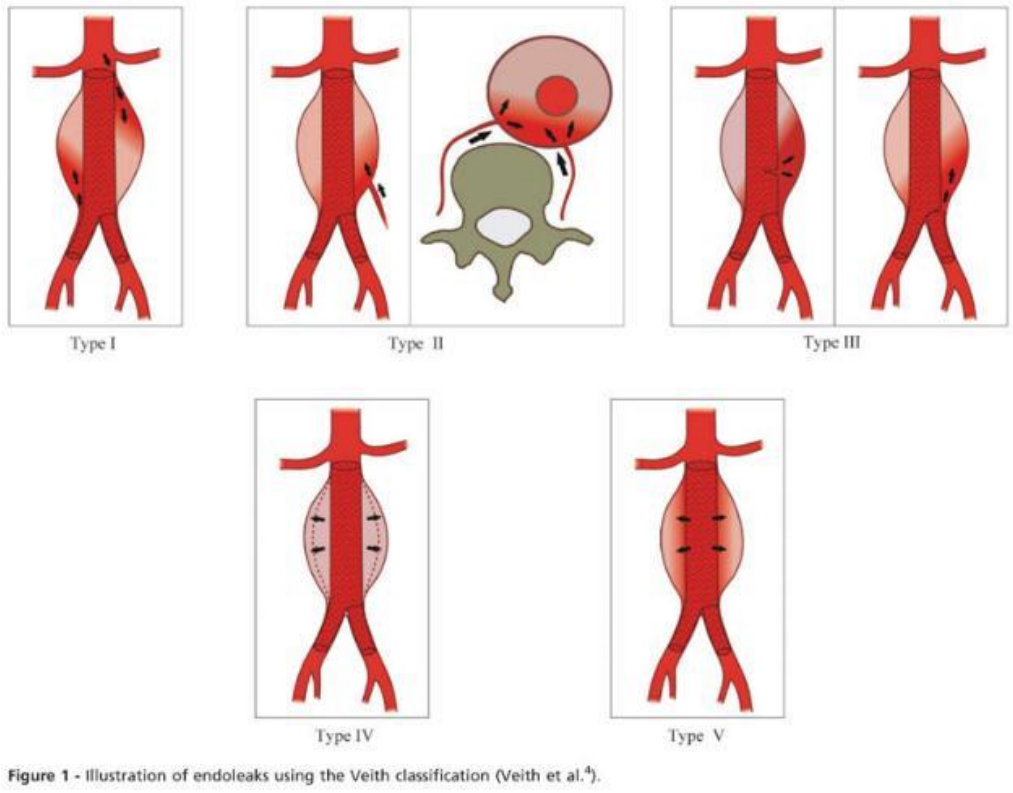

Figure 8: Illustration of the five different kinds of endoleaks (including endotension) [31].

Type I endoleaks can be repaired several different ways. If the leak is large, the surgeon may choose to reintervene and deploy an extension to provide sufficient fixation. However,

there must be a sufficient neck length (distance between the top of the aneurysm and the renal arteries) for this to be an option if the leak occurs on the proximal end. If this is not an option, the surgeon may choose to embolize the leak using glue or coils [33]. The issue with this treatment is that there can be recanalization at that site. If the endoleak is persistent, the aorta can be partially clamped; however this procedure is highly invasive and can have 30-day mortality rates up to 30%. The surgeon may also chose to do a conversion to open repair.

Type II endoleaks can be repaired via a transarterial approach or a translumbar approach [32]. The vessels most commonly responsible for these kinds of leaks are the inferior mesenteric artery and the lumbar arteries that branch off from the aorta. The first approach involves embolizing the aneurysmal sac, then embolizing the vessel responsible for the leak, both using either nitinol or stainless steel coils. The translumbar approach embolizes the endoleak sac nidus, which cuts off the blood flow between the arteries supplying the leak. This also uses stainless steel or nitinol coils, and is generally considered to be a more durable solution [34].

Type III endoleaks require a new stent-graft component to be deployed across the defective area. Type IV endoleaks are usually only seen immediately post-deployment as the patient is on high doses of the anticoagulant heparin for the duration of the surgery. This will resolve itself once the patient is no longer on heparin. Type V endoleaks generally require conversion to open repair.

2.7.2 Ruptures

Ruptures are tears or holes that form in the aneurysm, causing arterial blood to leak into the abdominal cavity. Approximately 15,000 people die a year from ruptured AAA, with

the frequency of rupture being 4.4 cases per 100,000 people [35]. The prognosis for a patient with a ruptured AAA is low. The initial mortality rate for patients whose ruptures occur outside of a hospital setting is approximately 50%, and the survival rate decreases nearly 1% per minute [35]. Ruptures are believed to occur when the wall tissue strength is exceeded by the mechanical stress acting on the aneurysm wall. This tension can be calculated using the Laplace Law for wall tension:

$$WT = PxR/W$$

Where WT= Wall Tension, P=mean arterial pressure, R=radius of the vessel, and W= wall thickness of the vessel. It can be seen from this equation that there is a positive relationship between the radius of the vessel and wall compliance, and since there is a higher risk of rupture with higher wall tension, it can be inferred that there is also a positive relationship between vessel radius and risk of rupture. The annual risk of rupture based on vessel diameter is outlined in Table 2.

Table 2: Estimated Annual Risk of Rupture based on Size of Aneurysm [35]

AAA Diameter (cm)	**Rupture Risk (%/y)**
< 4	0
4-5	0.5-5
5-6	3-15
6-7	10-20
7-8	20-40
>8	30-50

2.8 Devices

2.8.1 Medtronic Endurant

The Medtronic Endurant® Bifurcated Stent graft was approved for commercial use by the FDA in December 2010 [36]. It consists of two components, the main bifurcated body and the contralateral limb (See figure 9 for completed graft). The main body consists of a multifilament polyester fabric coupled with laser cut nitinol stents, sewn together using polyester sutures There is a bare nitinol stent affixed to the proximal end of the main body using ultra high molecular weight polyethylene sutures. This stent allows the device to be fixed above the renal arteries without preventing arterial blood flow to the kidneys, and as such is referred to as the suprarenal stent. There are barbs on the top of the suprarenal stent's stents to assist in anchoring the device to the aorta and prevent future migration. On the distal end, the main body bifurcates into the ipsilateral iliac limb and a contralateral stub. The contralateral stub has the stents sewn on the inside of the fabric to aid in securing the limb extension that will be deployed inside of it.

The contralateral limb component is deployed separately. It is designed to be oversized 10-25% compared to the iliac artery's inner diameter to ensure affixation and reduce the risk of endoleak. It is also flared on the proximal end in an open web configuration for the same reason. The friction between the inside of the contralateral stub and the outside of the contralateral limb is all that joins the two together, so the oversizing is key to ensuring a proper fit.

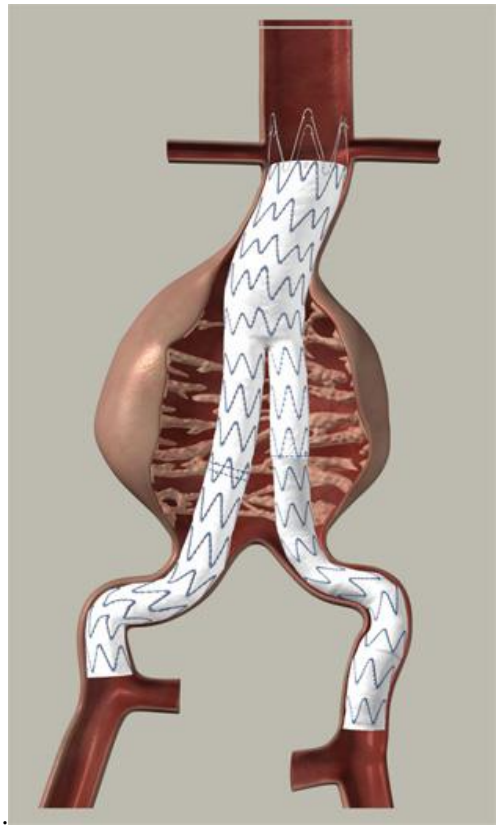

Figure 9: Shows Medtronic Endurant deployed inside an abdominal aortic aneurysm [37].

2.8.2 Clinical Behavior

An article by Makaroun et al shows the behavior of the Medtronic Endurant Stent Graft System after one year in the United States regulatory trial. 150 patients (primarily elderly males with significant comorbidities) with infrarenal aortic aneurysms were treated with the Endurant stent graft system. The inclusion criteria for this study were that the diameter of the aneurysm had to be larger than 5 cm, the proximal neck longer than 10 mm, the bilateral iliac fixation length longer than 15 mm, and the angle of the neck smaller than 60 degrees. Most of these are

concurrent with the instructions for use for the Endurant system [38]. The goal of this study was to examine the effectiveness of the system in preventing major adverse events and in successfully treating aneurysms after 12 months *in vivo* [39].

They found that 99.3% of the patients had a successful implantation. The patient who didn't had an incompatible iliac anatomy for the delivery system. After one month there was no operative mortality and only 4% of patients experienced major adverse events. 28.7% of patients experienced serious adverse events, the most frequent being cardiac, fever, urological, pulmonary, and vascular events in descending order in terms of frequency. After 12 months there was no evidence of migration or ruptures, and only 11.6% of patients had endoleaks (all Type II except for one Type I). Ten reinterventions had to be performed, for limb thrombosis/stenosis or to fix the endoleak. The sac diameter either remained stable or decreased for all patients. Seven patients died but none from aneurysmal complications. Makaroun et al concluded that these early results are encouraging and suggestive of a safe and effective device.

A more recent study by Setacci et al looked at the efficacy of the Endurant system in patients with a challenging neck anatomy, i.e. too short or wide, thrombus lined, highly angulated, or conically shaped. None of these patients meet the criteria for use described in the Endurant's instructions for use because a reliable seal and fixation is difficult to achieve. The study used 72 challenging patients and 65 control patients who had an average longer neck length and smaller infrarenal and suprarenal neck angle. Their short term results were promising with 100% technical success, similar rates of major adverse events between the test

and control group (1.54% and 1.39% respectively), and only 4 reinterventions needed to add a proximal extension to the implanted graft [40].

Torsello et al also compared the use of the Endurant in off-label conditions versus use according to the instructions for use. The patients chosen for the off-label use were all nonoperative candidates, or at a high risk for surgical repair. 121 patients were treated according to the IFU, 56 off-label. Technical success (successful implantation of the device) was seen in all but two patients. Clinical success was defined as a lack of aneurysm rupture, expansion more than 5 mm, Type I or III endoleak, infection or thrombosis, and death. This was achieved in 96.7% of IFU group patients and 96.4% of OL patients (all of the ones who had technical success). There was one aneurysm-related death in the OL group as a result of rupture from a Type I endoleak. Otherwise there was no significant difference in mortality at one year between the groups, and freedom from device-related reintervention and freedom from graft thrombosis rates were similar between the two groups. The authors concluded that while the early and intermediate results for the two groups were similar in terms of survival, major complications, and reinterventions, the risk for type I endoleak was higher in off-label uses and therefore caution should be applied when using this device off-label [41].

2.8.3 Cook Zenith

The Cook Zenith® AAA Endovascular Graft was approved for use by the FDA in May of 2003 [42]. It is in three different pieces, the main graft module, the contralateral limb module, and the ipsilateral iliac extension (See Figure 10 for the complete graft). All of these are constructed

with a full-thickness woven polyester fabric attached to self-expanding stainless steel Cook-Z® stents with a braided polyester and monofilament polypropylene suture. The distal end of the main body has a bare stainless steel stent designed to allow suprarenal fixation without disrupting blood flow through the renal arteries. The stent also has hooks on each stent spaced 3mm apart that are meant to dig into the aortic wall and prevent migration (see Figure 11). The top stent on the distal end, not including the bare stent, is sewn onto the inside of the fabric rather than on the outside like the remainder of the stents. The reason for this is to create a better seal. The distal end of the main body bifurcates into the ipsilateral iliac limb and the contralateral stub, similarly to the Medtronic Endurant® [43].

Both ends of the ipsilateral iliac extension have the last stents sewn inside the lumen to create a better seal when deployed. The contralateral extension is made the same way, and also flares out at the bottom to prevent endoleaks and create a better seal.

Figure 10: The Cook Zenith Flex ® Stent Graft with all components assembled. The contralateral limb is on the left in this image. [44]

Figure 11: Showing the suprarenal stent with hooks [44].

2.8.4 Clinical Performance

Bos et al looked at the performance of the Zenith graft in Europe between 1999 and 2006. 234 patients were included, with a mean aneurysmal diameter of 60.9 +/- 10 mm, and a neck length range from 10mm to 100mm, 44% being between 10 and 20 mm [44]. The technical success rate was 95.3%, but most of those patients did obtain technical success after additional components (limb and proximal extensions) were added. At 30 days the mortality rate was 1.7% due to myocardial infarctions and one cerebral hemorrhage. There were 28 mild, six moderate, and five severe surgical complications in 16.7% of patients, and three reinterventions were required within the hospital stay. The survival rates at each year are as

follows: 92.2 +/- 1.8% at one year, 87.2 +/- 2.3% at two years, 81.1 +/- 3% at three years and 69.9+/- 4.6% at five years. However, only four of the 43 patients who perished had deaths that were possibly related to aneurysmal complications. 50 patients total experienced endoleaks with 7 of them being high pressure type I or type III endoleaks. Both type three endoleaks were from disconnections of the contralateral limb, not from a defect in the graft fabric. The authors concluded the device to be safe based on low surgical mortality and a high secondary success rate. They also concluded the durability of the device in terms of mortality and reintervention rates at mid and long term follow-ups to be excellent [44].

Mertens et al looked at the long-term results of patients treated with the Zenith stent-graft. They analyzed 143 patients for overall survival, intervention-free survival, aneurysm rupture rates, early and late postoperative complications and endoleaks. At five years, 72.1% of patients had survived, and at 8 years 50.9% survived. By eight years 9% of patients (six total) had experienced a late aneurysm rupture, with three fatalities. 47 patients experienced endoleakage, 18 having type I, 25 with one or more type II endoleaks (33 total cases) and three type III, one of those requiring a conversion to open repair and another requiring a bypass, indicating a defect in the stent graft material rather than an incomplete seal between the limb stubs and extensions. There was also one case of endotension and 6 cases of stent fracture. The authors in this study concluded that the Zenith endograft is an excellent device with good long term results and low aneurysm related mortality [45].

2.8.5 Pre-fenestrated devices

Currently there is only one pre-fenestrated endovascular stent graft system approved for use in the United States. It is an iteration of the Cook Zenith® called the Cook Zenith Fenestrated®, approved for use by the FDA. It is custom made for each patient based on their personal aortic anatomy. This requires detailed CT scans of the abdominal aorta to properly locate the renal arteries and the superior mesenteric artery. The device is then manufactured with holes in the top piece for the renal arteries and a scallop at the top for the superior mesenteric artery (See figure 12) [46]. Though not indicated in the instructions for use, the fenestrations are occasionally supported by a nitinol metal ring sewn around the circumference of the fenestration, as seen through an image in a study by Halak et al (See figure 13) [47].

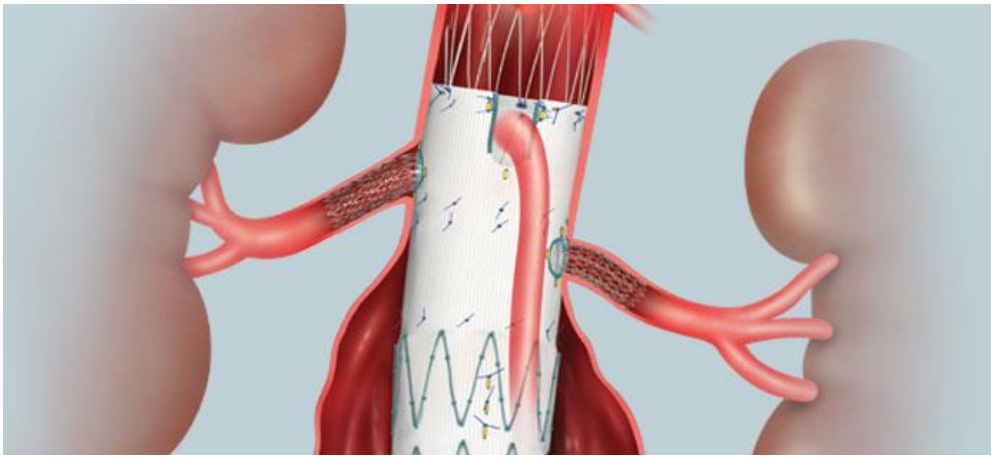

Figure 12: An illustration of the Cook Zenith Fenestrated deployed in an abdominal aorta [44].

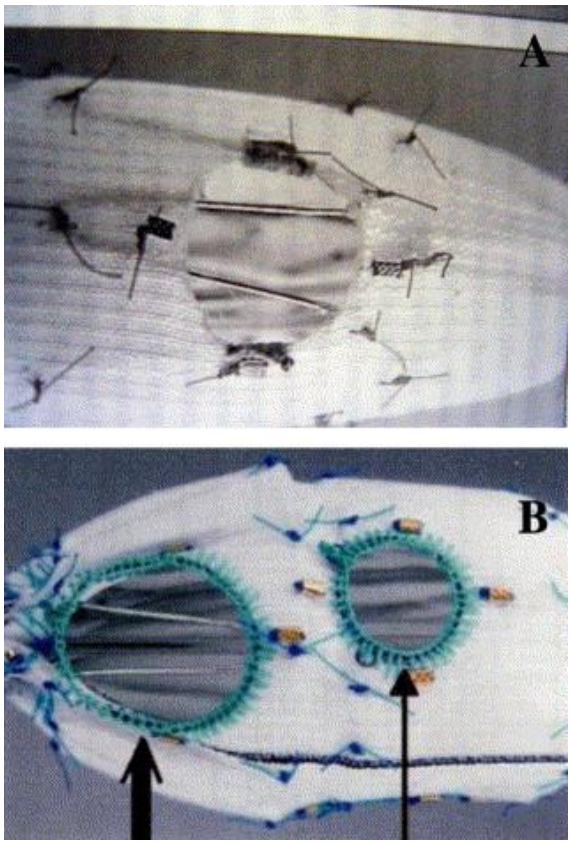

Figure 13: An image from a study on the fenestrated Cook endograft showing fenestrations both unsupported and supported by a nitinol ring [47].

The device comes in three parts, the proximal body graft with the fenestrations and scallop, the main bifurcated body graft, and the contralateral limb. All three are made out of a plain weave polyester fabric with extra yarns floated in the warp direction [15]. Stainless steel stents are sewn to the tubes with polyester and polyethylene sutures. Radiopaque markers are placed at various points along each part to aid in visualizing during fluoroscopy. The proximal body graft has the same suprarenal stent with barbs as the regular Zenith system. The two most proximal stents besides the suprarenal one are sewn to the inside of the lumen to aid in properly sealing the device to the aorta [48]. The main bifurcated body is nearly identical to the regular

Zenith system with the exception that there is no suprarenal stent and the most proximal stent is sewn to the outside of the graft. The contralateral limb is exactly the same as in the normal Zenith system.

2.8.6 Clinical Performance

Despite the recent release of the device, there have been several clinical trials on its patency. Correa and Oderich looked at the use in an 80 year old woman with a juxtarenal aneurysm 6 cm in diameter and growing. There were no complications during surgery, and no endoleak or complications after 18 months [49].

Greenberg et al looked at the intermediate results of the US trial for the fenestrated graft to evaluate the safety and short-term effectiveness of the device. 30 patients with short proximal necks were enrolled in the trial and treated with the Cook Zenith custom fenestrated devices. None of the visceral arteries, renal or superior mesenteric, were lost as a result of the surgery. After 24 months there were no aneurysm related deaths, ruptures, or conversions to open surgeries. There were 6 incidences of Type II endoleak at 12 months and 4 at 24. All patients had the diameter of the aneurysm either stay relatively the same (no growth greater than 5 mm). Eight of the 27 patients available for follow-up did experience a renal artery related event (4 stenoses, 2 occlusions, and 2 infarcts) and five had to undergo secondary interventions. However, none required dialysis and the authors concluded that the concept of fenestrated stent graft placement is safe and effective as long as the centers have experience [12].

Halak et al also looked at the use of the Zenith fenestrated endograft in 17 patients with 35 target vessels. The superior mesenteric artery required scallops in 7 patients and a small

fenestration in one, indicating a suprarenal aneurysm in the last patient. The main renal artery required 8 scallop fenestrations and 18 small fenestrations. Four kidneys had atrophic failure associated with the stenting. One was due to being unintentionally covered. Two kidneys were lost in one patient whose aneurysmal neck was severely angulated to the point that no access could be made to one renal artery and the superior mesenteric artery. An endoleak occurred on the proximal end and attempts to control it caused blood flow to be blocked to both renal arteries. The last kidney was found to have atrophied during follow-up. Overall only one patient required permanent hemodialysis. The authors concluded that accurate positioning intra-operatively is crucial to avoid compromising the target vessels and that post-procedural migration is a serious concern. However, they also expressed concern that mandatory stenting through the fenestration into the target vessel, though preventing device migration, would cause damage to the vessel leading to stenosis or thrombosis [47].

Two larger studies were done in Europe using the Cook fenestrated endograft, one in France and one in The Netherlands. The Netherland study, conducted by Verhoeven et al had 100 patients with 275 target vessels, comprised of 192 renal arteries, 78 superior mesenteric arteries, and five celiac arteries. Most of the target vessels in this study were stented through the fenestrations with either covered or uncovered stents depending on the anatomy of the patients [50]. The technical success rate of this (as in, the ability to catheterize and stent the vessel) was 98.9%, three renal arteries not being able to have been catheterized. Surgical mortality was only one patient due to mesenteric ischemia. Survival rate estimations at 1, 2 and 5 years are as follows: 90.3 +/- 3.1%, 84.4 +/- 4.0% and 58.5 +/- 8.1% respectively. These rates are lower than those experienced by the normal Zenith endograft, but the aneurysms

experienced are more severe [45]. Overall visceral branch patency at five years was 93.3 +/- 1.9%, and there was no loss of vessel patency after 24 months. Of the 12 patients and 13 vessels that became occluded, four were due to malpositioning, reinforcing the importance of proper deployment [50]. While the authors concluded that fenestrated EVAR surgery is promising, it should be noted that 25% of the patients experienced a decrease in renal function [51].

The other major European study in France was conducted by Amiot et al was larger and had more positive outcomes than the Verhoeven study. 134 patients with 403 visceral vessels were treated with a fenestrated Cook device. 265 of the vessels were renal arteries. 99% of the target vessels were patent after surgery. The five exceptions were a distal implantation of a covered renal stent totally occluding all renal branches, a mistaken implantation into an accessory renal artery instead of the main renal artery, failed catheterization of two renal arteries that were already stenosed tightly, and failed catheterization of a celiac artery due to compression by an adjacent ligament. The 30 day mortality rate was 2%, two patients out of the three having complications leading to multisystem organ failure. The postoperative renal function is outlined in Table 3.

Table 3: A table from a study by Amiot et al showing renal function after surgery [52]

	Decrease *N* (%)	Increase *N* (%)	Stable *N* (%)	Temporary dialysis *N* (%)	Permanent dialysis *N* (%)
Preoperative renal insufficiency (eGFR < 60 ml/min) (*n* = 53, 40% of patients)	8 (15)	14 (26)	32 (59)	3 (5.5)	1 (2)
Normal preoperative renal function (eGFR> 60 ml/min) (*n* = 81, 60% of patients)	5 (6)	10 (12)	66 (82)	1 (1)	1 (1)
All	13 (10)	24 (17)	98 (73)	4 (3)	2 (1.5)

The mortality rate at 24 months was 86%; however, none of these deaths were complications from aneurysms. The majority of the endoleaks found in follow-ups were type II. There was one example of a type III endoleak resulting from the fenestration. However, this fenestration had not been stented due to renal stenosis and a resulting inability to catheterize. The four incidences of renal artery occlusion found in follow-ups did not result in a need for hemodialysis. Overall there was a decrease in renal artery performance in 10% of patients [51-52].

2.9 Novel approaches to treatment of pararenal aneurysms

Though the Cook Zenith Fenestrated® has shown decent potential in a number of studies [48 50, 51, 52, 54], it has a significant limitation in the amount of time required to produce the device. Each one is custom made based on detailed CT scans of the patient's abdominal aorta. While this does allow for increased accuracy of fenestration placement, the success of the device requires that the patient's anatomy remain stable until the device can be acquired. It can take between 6-12 weeks for the device to be manufactured, and there is no guarantee that the patient will be able to wait that amount of time, nor that their aortic anatomy

will remain unchanged [9-12]. Therefore, a significant emphasis has been put on researching methods of fenestration that can be done on-site or *in-situ*.

Oderich et al modified a TX2® Cook Medical off-the-shelf pre-fenestrated device by adding reinforced mini-cuffs to the fenestrations. This was done on-site in the operation room. An 8-mm Viabahn stent graft (W. L. Gore, Flagstaff, Ariz) was cut into 3-5 mm long pieces then sewn onto the fenestrations using Ethibond sutures (see Figure 14). The fenestrations were for the superior mesenteric artery, the celiac artery, and the right renal artery, as the patient's left renal artery had been bypassed during a previous open repair. The device was then deployed and the gap between the vessels and the mini-cuffs were each bridged using three different stent grafts deployed inside each other at intervals to reinforce each other and prevent kink. After completion the target vessels were patent and there was no evidence of endoleak [9].

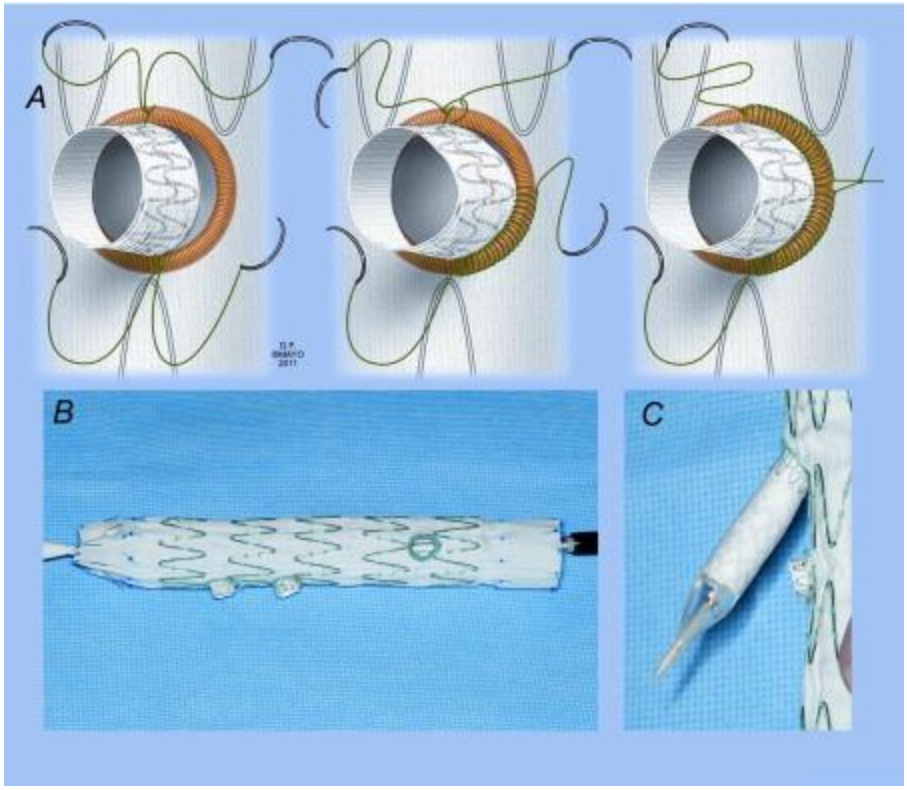

Figure 14: Image from Oderich et al showing mini-cuff reinforced fenestrations [9].

Tse et al created a custom structure for a patient by attaching three branches to a device that would be connected to the celiac, superior mesenteric, and right renal arteries. The dimensions and positions of each of the arteries were determined at a previous point using CT images and angiograms. The methods used to create the fenestrations and attach the branches (made of cut vascular grafts) were not outlined, but presumably it was done by deploying the stent graft, creating the fenestrations and attaching the branches, then reinserting the modified graft into the delivery system. The branches were connected to their intended arteries using

additional stents. At 8 months after the device was successfully implanted, all of the target arteries remained patent and the size of the aneurysm had decreased [13].

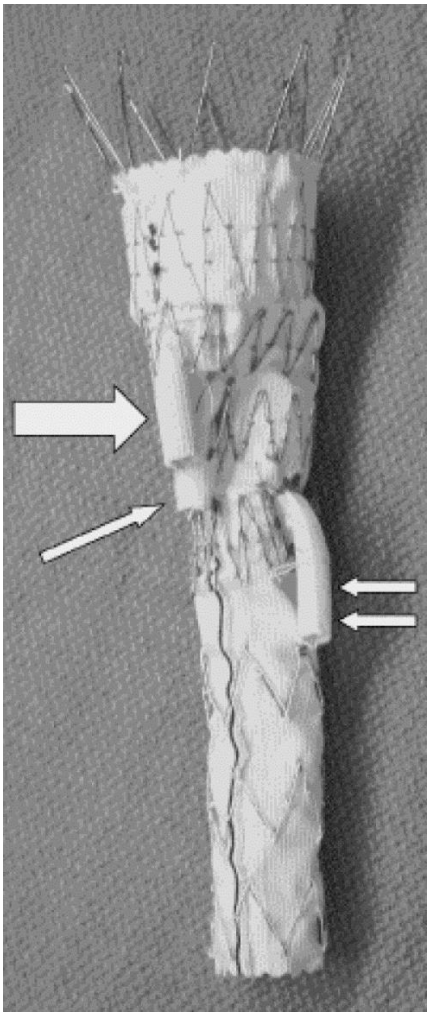

Figure 15: The branched custom structure created by Tse et al. The large arrow is the celiac branch, the small arrow the superior mesenteric branch, and the double arrows the renal branch [13].

Dr. Leonard Tse and other co-others also looked at an *in situ* fenestration technique to prevent occlusion of the renal arteries after the deployment of an endovascular stent graft. It

was tested in two large canines, not in humans, using an iliac extension as the endovascular stent graft. The fenestration was done using fluoroscopic guidance and the puncture made with a Brockenbrough needle. The device was explanted after one month and analyzed, focusing on fabric tearing. Only one dog was able to be used for the experiment in the end, and technical success was achieved in both renal arteries. Patency was observed after one month in both renal arteries as well. Once the device was explanted, there was no evidence of damage outside of the fenestration area. The authors concluded that while the procedure was technically feasible, improvements are required for it to be a reliable and reproducible procedure [14].

2.10 Material Performance

It is important to be able to understand the performance of the materials that make up the components of the stent graft so that its performance in off-label uses can be properly compared. The previous research that this thesis was based off of involved the use of in situ radiofrequency (RF) puncture of the endograft fabric and subsequent angioplasty ballooning of the fenestration to the desired diameter. The primary goal of this initial study was to determine the effect of this procedure on the long term mechanical, dimensional, and geometric performance of the endograft material [15].

The five materials used in this study were: (1) a monofilament twill woven polyester fabric (Medifab) chosen to represent the Talent™ graft material, (2) a multifilament tubular woven polyester fabric (Atex) representing the graft component of the Zenith device, (3) a multifilament plain woven tubular polyester fabric used in the Endurant device, and (4 and 5)

two types of expanded polytetrafluoroethylene (ePTFE) membranes, Standard and Next Generation (Zeus Inc., Orangeburg, SC) [15].

The fabrics and membranes were first punctured using a radiofrequency puncture generator and were then gradually ballooned using a series of 2.5, 5, and 7 mm balloon catheters sequentially. Tests were performed on both fenestrated and unfenestrated control specimens to measure their microscopic appearance (SEM), fabric dimensions, woven fabric count, tearing strength, and probe bursting strength. The fenestrated specimens were also monitored for defects, fenestration measurements, and fatigue resistance testing [15].

For all of the woven fabrics there was fraying around the edges of the ballooned fenestrations. For both the Atex and the Endurant samples some of the yarns around the edges of the RF puncture site melted, fused together and encroached on the fenestration site (Figure 16). The Medifab fabric did not show evidence of this, possibly because it was woven with a monofilament yarn. The Atex fabric did not expand very much after ballooning, which correlated with its significantly higher bursting and tearing strength. It did show a 75% increase in the RF punctured fenestration area as a result of fatiguing. The Medifab fabric also showed a 31% increase in the fenestration area after fatiguing and had the lowest tearing and bursting strength of all three woven fabrics. The Endurant showed no change in fenestration area, performing at an intermediate level between the Atex and Medifab fabrics for tearing and bursting strength [15].

Both ePTFE fabrics showed less melting around the edges of the ballooned fenestration, possibly because the melting point of PTFE had not been reached. The Standard ePTFE had no change in tearing strength as a result of fenestration, whereas for the Next

Generation ePTFE sample there was an increase in longitudinal tearing strength after fenestration [15].

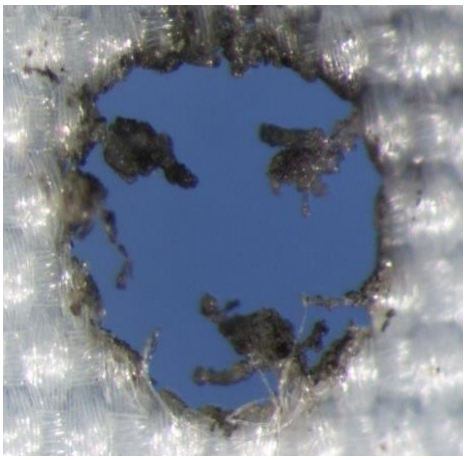

Figure 16: Endurant fabric showing melted and fused fibers encroaching after RF puncture and ballooning [15].

It was concluded from this initial study that the type of fabric and membrane, as well as their construction, play a distinct role in the material's performance after fenestration. Additionally, the various materials exhibited significant changes in their dimensional, geometric and mechanical characteristics as a result of in situ radio frequency (RF) puncture and balloon expansion [15].

King et al looked at the microstructural behavior of polyester textile implants in humans. Thermal analysis, FTIR spectroscopy, and vapor phase dyeing techniques were used to categorize any changes in the microstructure of polyester explants (in vivo for 2-16 years). They found that the slow biodegradation of polyester fibers is in fact a multi-step process that

starts with fiber swelling and molecular chain scission, continues with the loss of surface amorphous material, and ends with the reorganization of the microcrystalline structure through the larger crystalline regions, sacrificing the smaller crystalline regions and amorphous regions. The authors concluded that the resulting structure was likely to show an improvement in resistance to subsequent degradation [53].

Guidoin et al analyzed explanted Stentor devices from the EUROSTAR registry. The Stentor is a first generation aortic endograft. Six devices, in vivo for 13 to 53 months, were explanted and analyzed for changes using radiography, endoscopy, MRI, histology, SEM, and electron spectroscopy. They found evidence of yarn distortion, damage, and filament breakage in the polyester fabric which led to the formation of defects or holes. The thrombotic matrix showed evidence of incomplete healing. The failure of the grafts was due to the metal stents. The sutures tying them to the polyester broke, and subsequently they were dislocated and compacted. The NiTi stents additionally showed evidence of corrosion and non-homogenous surface chemistry. The authors concluded that the assembly of the device required significant improvement [54].

Riepe et al also analyzed the in vivo alterations of polyester vascular grafts in humans. They wanted to see if the hydrolysis experienced in vivo by the polyester grafts had an impact on the physical properties, and if there was a correlation to the time passed in the body. There were 65 explanted grafts ranging from 0-23 years in vivo. Probe puncture, infra-red spectroscopy, and SEM were performed to measure the physical strength, the molecular integrity, and the surface, respectively. They found evidence of scission of macromolecular chains and evidence of loss of physical strength due to the correlation of time spent in the body

and hydrolytic degradation. A linear regression analysis showed a 31.4 % loss in bursting resistance in 10 years. After 25-39 years, the loss increased to 100% [55].

A co-author, Chakfé, on the previous study led another study on a similar topic, this time looking at the influence of the textile structure on the degradation of aortic endoprostheses. 31 samples, a mixture of Stentor, AneurX, Talent, and Vanguard devices, were explanted and subjected to optical microscopy, SEM, filament dynamometry, and saturation index measurement. The results showed macroscopic lesions on the Stentor, Vanguard, and Talent devices. The lesions on the first two appeared to be holes at the stent extremities and warp yarn slippage due to proximity to sutures or seams. The lesions on the Talent devices seemed to be a result of abrasion. Significant polymer degradation was not observed; however the authors concluded that further studies are needed to confirm that data [56].

CHAPTER 3: METHODS AND MATERIALS

3.1 Design of Experiment

This experiment was designed to identify and quantify the effects of two different kinds of fenestration on stent grafts that had been fenestrated then fatigued for the equivalent of one year *in vivo* on certain dependent variables.

3.1.1 Dependent Variables

The dependent variables are:

- Fabric count: The number of warp yarns and weft yarns per unit area of woven fabric.
- Probe bursting resistance: The minimum force required to burst a hole through the graft fabric with a probe.
- Macroscopic and microscopic appearance: The ability of the graft material to retain its appearance after fenestration and fatigue on a macroscopic and microscopic level.
- Fenestration size: The measured height and width of the fenestration area.

3.1.2 Independent Variables

The Independent Variables are:

- Stent Graft Selection:
    - Medtronic Endurant®
    - Cook Zenith Flex ®
- Fenestration condition
    - Control (no fenestration)

    - RF puncture and balloon angioplasty
    - RF puncture and cutting balloon
- Fatigue condition
    - Control (no fatigue)
    - Fatigued for 40,000,000 cycles at hypertensive pressure

3.3 Materials

3.3.1 Stent Grafts

Two different types of endovascular stent grafts were chosen based on recommendations by the two different surgeons involved in this project. The Cook Zenith is an older but well used and tested device. The Medtronic Endurant is a relatively new device put on the market to phase out the Medtronic Talent, an older device with some flaws. In addition to these endovascular stent grafts, eight Atrium ePTFE-covered stainless steel stent grafts were used to stent open the renal fenestrations.

3.3.1.1 Cook Zenith

The Cook Zenith, as described in section 2.83, is an endovascular stent graft with a modified plain weave polyester fabric component and stainless steel stents. The samples used are as follows:

- One 30 mm diameter 140 mm body length sample, used in GC2
- One 28 mm diameter 125 mm body length sample, used in GC1
- One 26 mm diameter 140 mm body length sample, used as control
- Two contralateral limbs
- Two iliac extensions

3.3.1.2 Medtronic Endurant

The Medtronic Endurant, as described in section 2.8.1, is an endovascular stent graft with a plain weave polyester fabric component and NiTi stents. The samples used are as follows:

- Three 25 mm diameter bifurcated main body grafts (one used for control)
- Eight 16 mm diameter iliac extensions

3.3.1.3 Atrium Stent Grafts

The Atrium Advanta™ V12 covered stents are balloon-expandable stents coated with ePTFE designed for use in the iliac and renal arteries [57]. The sizes used are as follows:

- Eight 6 mm diameter 35 mm length stent grafts

3.3.2 Phantoms

The plastic models that the stent grafts were deployed in were a modified version of a model designed by Louise Allard, Gilles Soulez, Boris Chayer, Zhao Qin, and Guy Cloutier [58]. Allard et al set out to create a realistic model of the abdominal aorta with a visible thrombus to potentially aid in future *in vitro* stent graft experiments and the improvement of deployment. They took detailed CT scans of a real patient with an abdominal aortic aneurysms and used imaging software to recreate a 3D epoxy resin model. A negative master mold was made out of silicone. A thrombus was built up using agar-gel and the final AAA phantom was enclosed in a polyethylene container and coated in polyurethane. The phantom was then dissolved out [58].

To make this initial design fit the Bose Pulsatile Fatigue Tester, it was necessary to create modifications to the design. The diameter of the main aorta and the shape of the

abdominal aneurysm were kept the same. The renal stubs from the original design were hollowed out and lengthened to create full renal arteries. The superior mesenteric stub was removed. The iliac limbs were made the same diameter and given enough length to attach to the ports on the fatigue tester. The biggest change was at the proximal aortic end. The aorta was split into two branches, similar to the iliac limbs, in order to be able to attach them to the fatigue tester. The initial model and the modified version can be compared in Figure 17. Four phantoms were manufactured based off of this design. It should be noted that due to the way the polyurethane was coated on, each phantom was slightly different. The overall anatomy of each was the same, but the wall thickness varied in certain spots. This combined with the different internal geometry of the four different stent grafts made it so that each device had to be tested slightly differently on the fatigue tester.

Figure 17: The initial model created by Allard et al on the left, two samples of the modified version on the right [58].

3.3.3 Baylis PowerWire™ Radiofrequency Guidewire

The fenestrations were performed using the Baylis PowerWire™ Radiofrequency guidewire. It is designed to disintegrate what it punctures through, and can additionally be used as a mechanical guidewire to push through a tough area [59].

3.4 Methods

3.4.1 Deployment

Each of the four stent grafts used in this study were deployed into one of the four phantoms according to the instructions for use for each device, but also taking into account the placement of the stent graft above the renal arteries. The deployment was done under fluoroscopy, to be as close to an actual surgery as possible.

3.4.1.1 Medtronic Endurant

Each of the Endurant stent grafts were deployed the same way, using the instructions for use and surgical experience as guidelines, under the operation of Dr. KT Tan and Dr. Leonard Tse of the University of Toronto Hospital. Dry conditions were used. Fluoroscopy was used to visualize the deployment, as the phantoms are opaque. A guidewire was advanced through one of the iliac limbs until it was above the renal arteries. The delivery system for the bifurcated main body was viewed under fluoroscopy to locate the radiopaque markers, then advanced over the guidewire into the phantom until the top edge of the fabric was above the renal arteries, placed right below where the superior mesenteric artery would have been in an actual patient. The graft cover was then slowly withdrawn as seen in Figure 18 (but placed above the renal arteries). The withdrawal was continued until the contralateral stub was fully

deployed, then paused. At this point the suprarenal stent was released. The deployment of the main body was then continued until the ipsilateral limb was fully deployed. The delivery system was then pushed up until no longer in contact with the suprarenal stent, and removed.

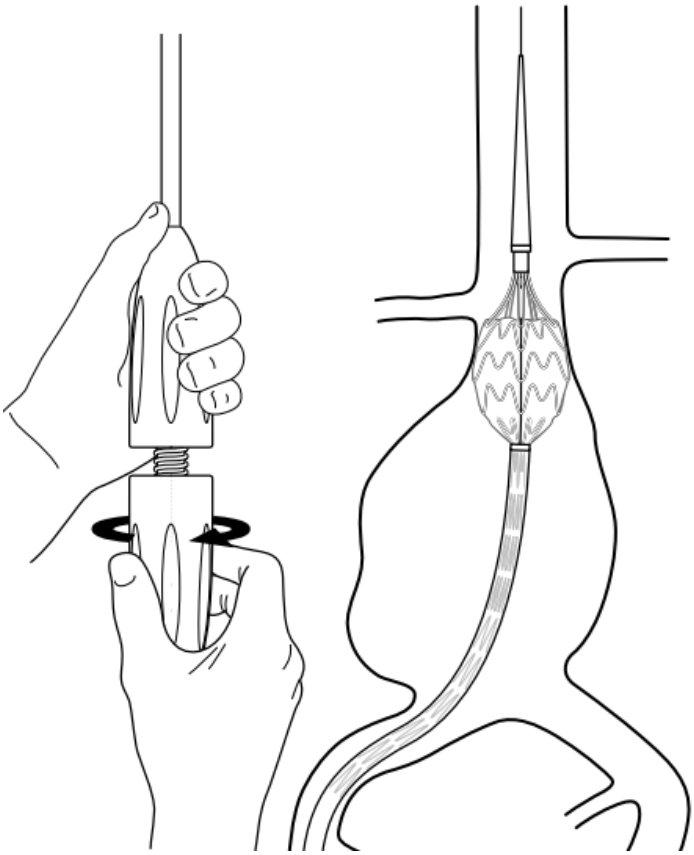

Figure 18: Shows one of the deployment steps according to the instructions for use [38].

The bifurcation in the body of the Medtronic Endurant occurs fairly high up, and as such several limb extensions had to be added. First the contralateral limb extension was added in a similar manner to the main body (skipping the suprarenal step), ensuring it was placed up

to the radiopaque markers at the top of the contralateral stub. Another extension was added to this to ensure that it would be long enough to reach into the phantom's limb, then another extension was added through the last two to ensure proper seal and add strength. On the ipsilateral side, an iliac extension was added to again ensure that the limb reached far enough into the ipsilateral limb of the phantom, then another through that and the ipsilateral limb to ensure a proper seal and again, add strength. This entire procedure was repeated with a second phantom.

3.4.1.2 Cook Zenith

Both Zenith grafts were deployed in the same fashion into the phantoms, relying on surgical expertise for the method. Like the Endurant devices, both of these were deployed under dry conditions using fluoroscopy. The operator was Dr. Mark Farber of UNC Hospitals. Sterile water was used to ease the process as the polyurethane created some friction that interfered with the insertion of the delivery system.

First a guidewire was inserted into the ipsilateral limb and forwarded through the entire device and out of one of the proximal branches of the phantom. This was done so that the guidewire could be held down, assisting the insertion of the delivery system. While this would not be done in an actual surgery, the friction experienced here due to the polyurethane would also not be experienced in an actual surgery; ergo, holding down the guidewire would not be necessary. The delivery system for the main body graft was then inserted and forwarded until the top edge of the fabric was above the renal arteries. The graft was then deployed until the contralateral stub was released. As with the Endurant, the suprarenal stents were then released. The ipsilateral limb was then deployed and the delivery system removed. At this point, an

extension was added to both the contralateral and ipsilateral limbs to secure them to the iliac limbs of the phantom. This procedure was repeated in the second phantom.

3.4.2 Fenestration techniques

Two different fenestration techniques were employed on the deployed stent grafts. The RF fenestration and subsequent angioplasty ballooning technique described by Eadie was employed in all four stent grafts, but in one of each type of stent graft (Endurant, Zenith), a cutting balloon was additionally used to score the fenestration open more and thus increase the final diameter of the fenestration. It was noticed by Eadie et al that the Zenith fabric, when fenestrated and ballooned, did not achieve the same diameter as the balloon, and in fact shrunk significantly once the balloon was removed [15]. Therefore it was decided to include a cutting balloon in this experiment to avoid the fabric clamping down on the renal stent and significantly reducing or even cutting off flow from the renal arteries.

After this point the devices were each given a different name for ease in telling them apart. GC1 is the Cook Zenith device fenestrated without a cutting balloon. GC2 is the Cook Zenith device fenestrated with the aid of a cutting balloon. GM1 is the Medtronic device fenestrated without a cutting balloon, and GM2 with a cutting balloon. The ‘G’ stands for ‘Georges’, which refers to the nickname given to the original design of the aortic phantom [58].

The radiofrequency puncture was done using a Baylis Radiofrequency Puncture Generator and PowerWire™ Radiofrequency Guidewire (See Figure 19) [59]. Both are specifically designed to create controlled punctures by vaporization using radiofrequency energy through occlusions during vascular surgery. The guidewire is flexible and able to be

manipulated into a shape and stay in that shape, convenient for a tortuous anatomy. It can also be used like a normal guidewire to be physically pushed through occlusions, which was useful in this study as the fabric, especially the Zenith graft fabric, turned out to be quite tough and need the mechanical force in addition to the radiofrequency energy to be fully punctured.

Figure 19: The Baylis Radiofrequency Puncture Generator

The phantoms were mounted one at a time into a custom made bath and filled at all ports with 0.9% Normal Saline (See Figure 20). The bath used the same ports designed for use on the fatigue tester and attached them to watertight seals that guidewires could be pushed through if necessary, which it was for this study. The grounding ring, necessary for the procedure, was inserted into the top left port. The actual fenestration was done under fluoroscopy to mimic actual endovascular surgery. The process for each device was slightly different, and as such each will be outlined separately. All operations were performed by Dr.

Kong Teng Tan and Dr. Leonard Tse of the Interventional Radiology/Vascular Surgery department at Toronto General Hospital.

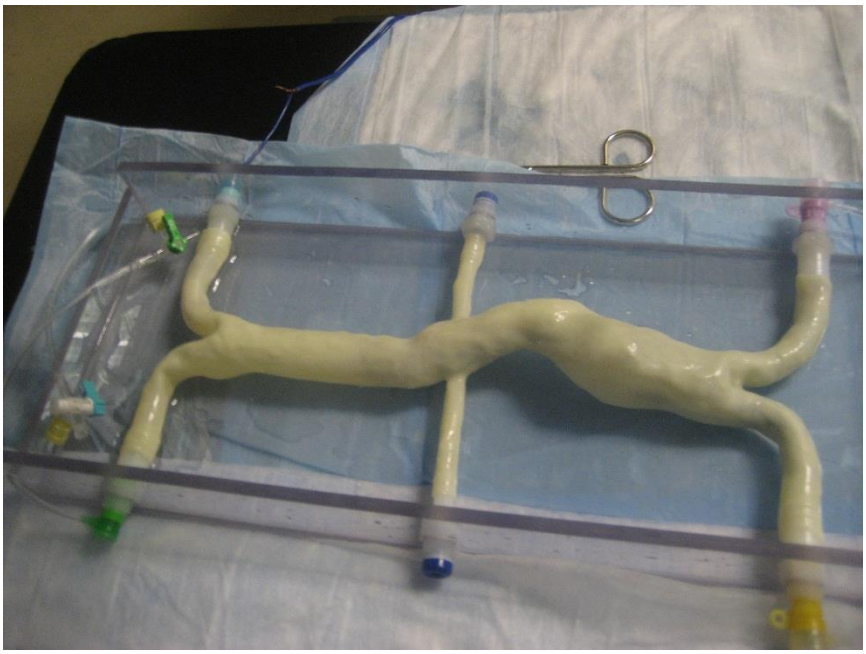

Figure 20: The custom bath with one of the phantoms mounted.

3.4.2.1 GM1

Once the fluoroscopy was set up to look straight down at the phantom, a curved guiding catheter was forwarded into the perirenal segment of the aorta. The radiofrequency wire and a five French catheter were then advanced up the juncture of the left renal artery and the aorta (left here referring to the patient's left, as is typical in clinical practice). The fluoroscopy unit was rotated to the side to confirm the orientation. The RF wire was attached to the generator and applied to the graft fabric on medium for two seconds, then high until puncture was achieved (approximately two seconds), and the RF wire was pushed into the renal artery and

through the port to ‘snare’ it. This was done because of the short length of renal artery available. A four French catheter was pushed into the renal artery, and the RF wire was exchanged for a regular guidewire (0.018”). A 3mm angioplasty balloon was inserted through the fenestration and dilated under manometer to 10 atm. No significant waist was seen, which is to say, the fabric did not pinch the balloon to a smaller diameter. The balloon was replaced with a 4mm balloon in the same position and dilated the same way, again not seeing a significant waist form. The 0.018” guidewire was replaced by a stiffer 0.035” support wire and a seven French curved catheter advanced up to the opening. It was not physically able to be advanced into the renal artery itself, so it was left in the aorta while the 6mm balloon-expandable Atrium graft was positioned so that two thirds were in the renal artery and one third was in the aorta. It was expanded under manometry to 16 atm, then 20 atm after a waist was seen. A waist still remained, and it was still impossible to advance the 7Fr sheath. A 10 mm angioplasty balloon was used to flare the end of the stent graft that remained in the aorta. This is done to prevent the renal stent from advancing further into the renal artery. The specimen was examined, and the procedure for the left renal artery was completed and all instrumentation removed. The right side was repeated in the same way but there were difficulties due to the short main body. A combination of several different catheters was required. Eventually the longer angled catheter worked. The finished deployment can be seen in Figure 21. Note the waists at the junctions of the renal arteries and the stent grafts.

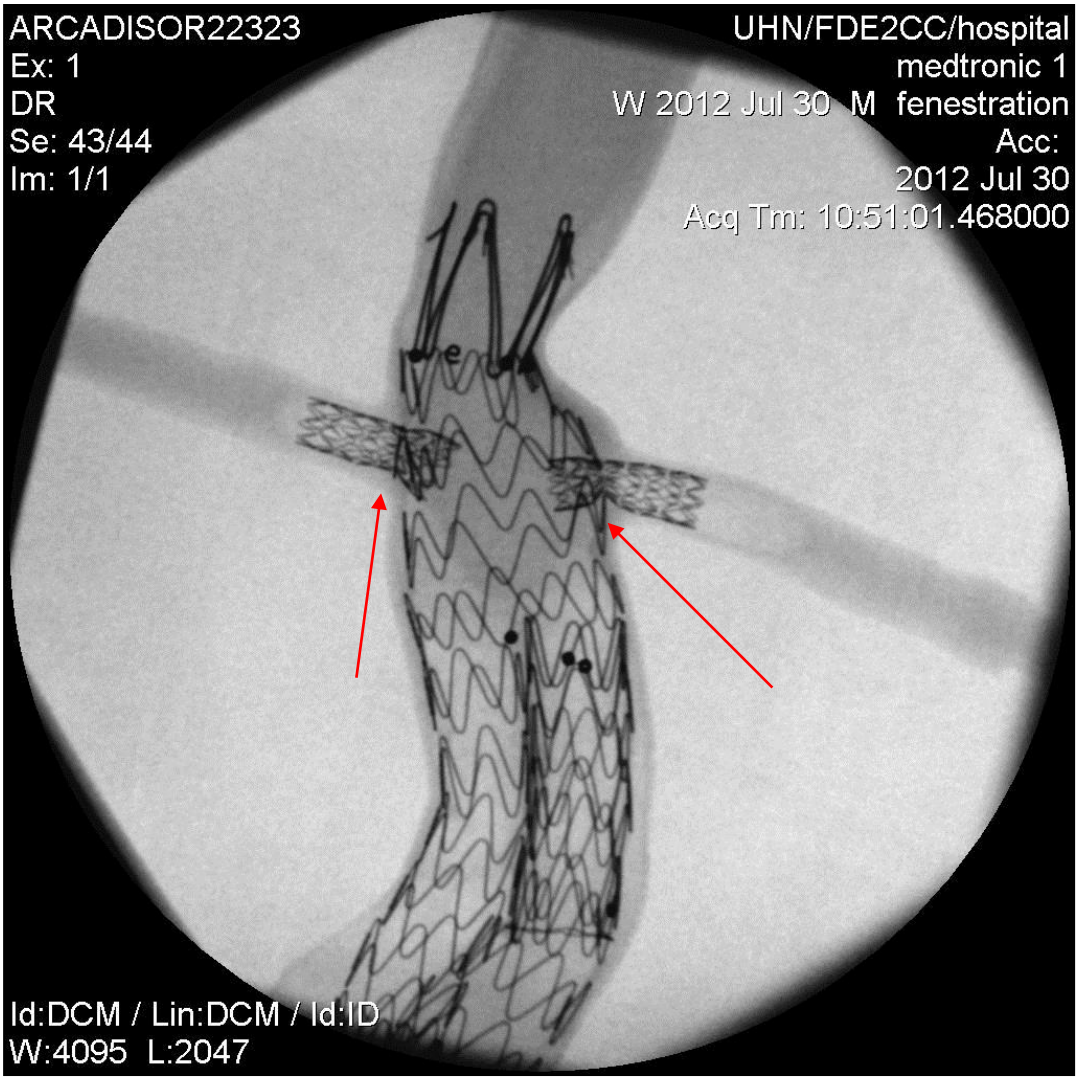

Figure 21: Finished deployment and fenestration of GM1 device. Note the waists, especially at the patient left renal artery.

3.4.2.2 GM2

The fenestrations on the second Medtronic device were performed in the same way as the first Medtronic device with several exceptions. The initial fenestrations were performed with the generator set on continuous/constant instead of pulsed high. In addition, the 4mm

conventional angioplasty balloon was replaced with a 4mm cutting balloon, which was expanded under manometer to 4 atm. The completion image can be seen in Figure 22. There is little to no waist that can be seen on this device.

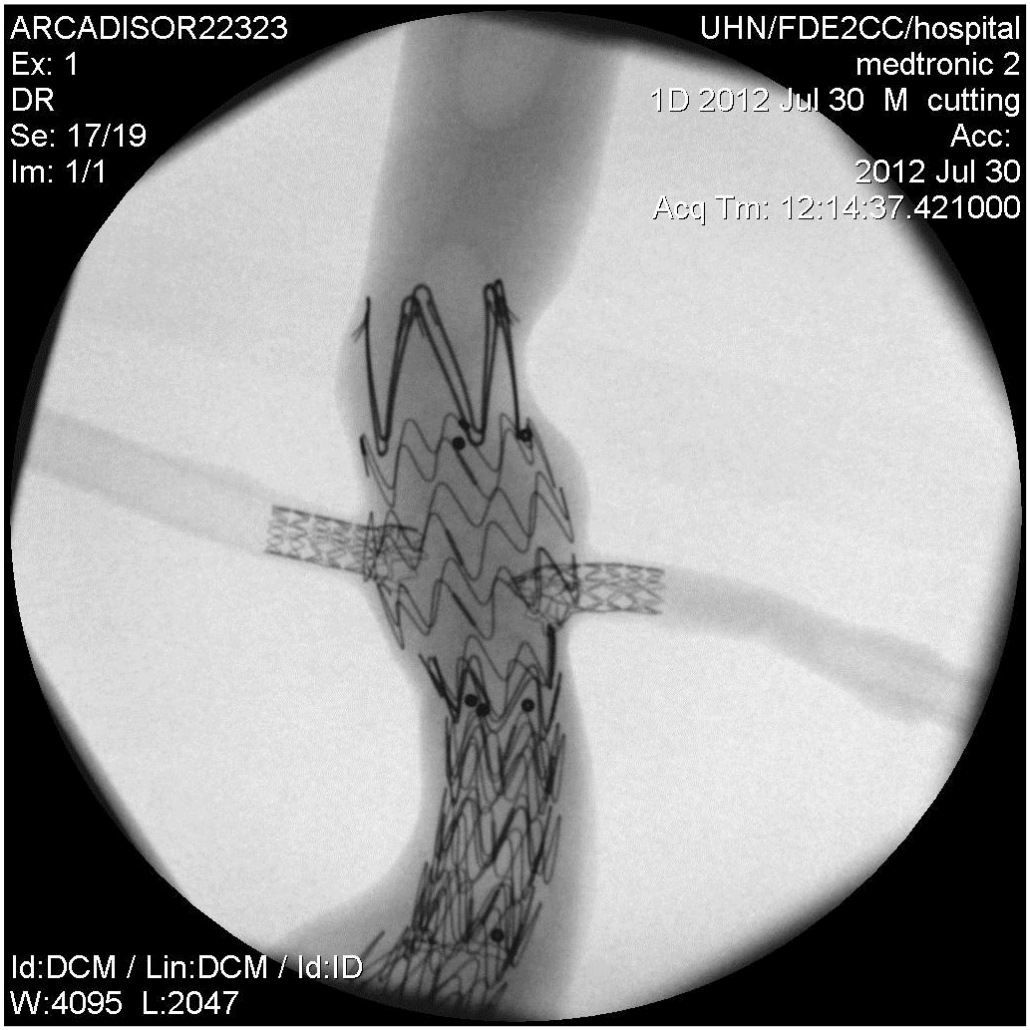

Figure 22: Completion image for GM2 device. Note the healthy waist on both renal arteries.

3.4.2.3 GC1

The fenestrations were performed the same way as the first Medtronic device, again with some aberrations. Two catheters had to be used together early on. The fenestrations were initially attempted with a high pulse cut, but after several failed attempts the generator was switched to continuous cut. At one point bubbling could be heard. Eventually, a successful puncture was achieved. The atrium stent was unable to be advanced through the fenestration, so a 7Fr dilator catheter was used first. After that the atrium stent was able to pass. The completion image for this device can be seen in Figure 23. Severe waists can be seen on both renal extensions.

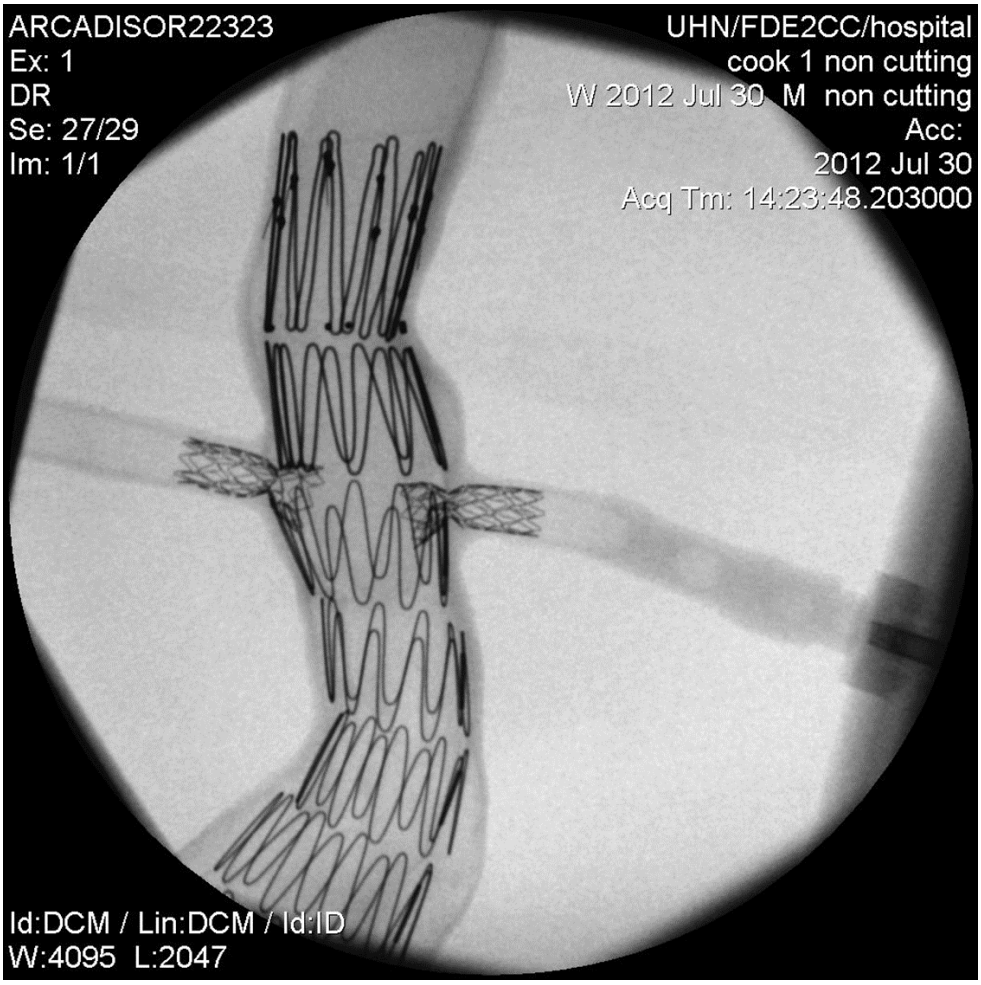

Figure 23: Completion image for GC1 device. Note the severe waists on the renal stent grafts.

3.4.2.4 GC2

The second Cook device also had the same technique performed, except that a 4mm cutting balloon replaced the 4 mm conventional angioplasty balloon as with the second Medtronic device. The radiofrequency generator was also set to continuous cut as for the previous two devices. No complications were seen with this device. The completion image can be seen in Figure 24. Healthy waists can be seen for both renal stent grafts. The patient left

renal extension showed a slight waist, but it may have been due to its position relative to the nearby stents.

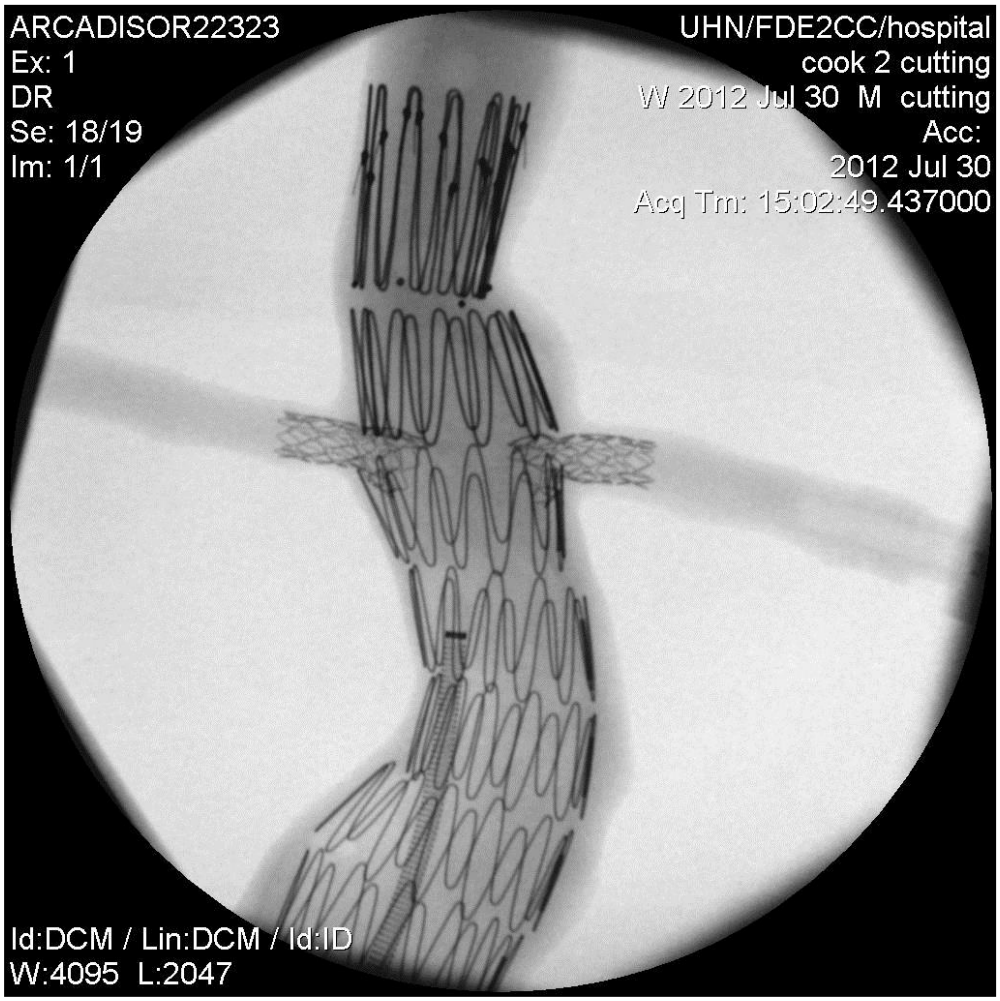

Figure 24: Completion image for GC2 device. Both renal arteries have a relatively healthy waist.

3.4.3 Pulsatile Fatigue

Each of the four devices were mounted on a Bose Enduratec SGT 9110 Pulsatile Fatigue Tester and cycled for 40,000,000 cycles. The average heart beats 1.2 times a second, and approximately 40,000,000 times in one year. Since the FDA requires test results at one year and ten years, the more achievable one year was chosen as the end point for each device. It was decided that each device should be tested at hypertensive pressures. While the link between hypertension and AAA is weak, many patients still present with hypertension as a comorbidity [4].

The Enduratec Pulsatile Fatigue tester works by attaching tubes between two manifolds containing water delivered from an external tank. Speakers attached to the manifolds displace water in and out of the tubes, creating a systolic and diastolic pressure. The rate at which this happens and the displacement are controlled by the WinTest software that accompanies the test system. The pressure is set by creating a waveform to control the displacement. To change the pressure, the displacement needs to be changed. In this study, a sine wave was used as it most closely mimics the behavior of blood pressure in the human body.

The devices were mounted vertically onto twelve different ports on the tester (see Figure 25). In order to ensure that they would not leak, the renal ports were covered with PTFE tape before the devices were mounted, and after the devices were mounted, each end was secured with a self-binding silicone tape. The tester was then filled with water and the machine rocked to release any air bubbles that would interfere with the testing.

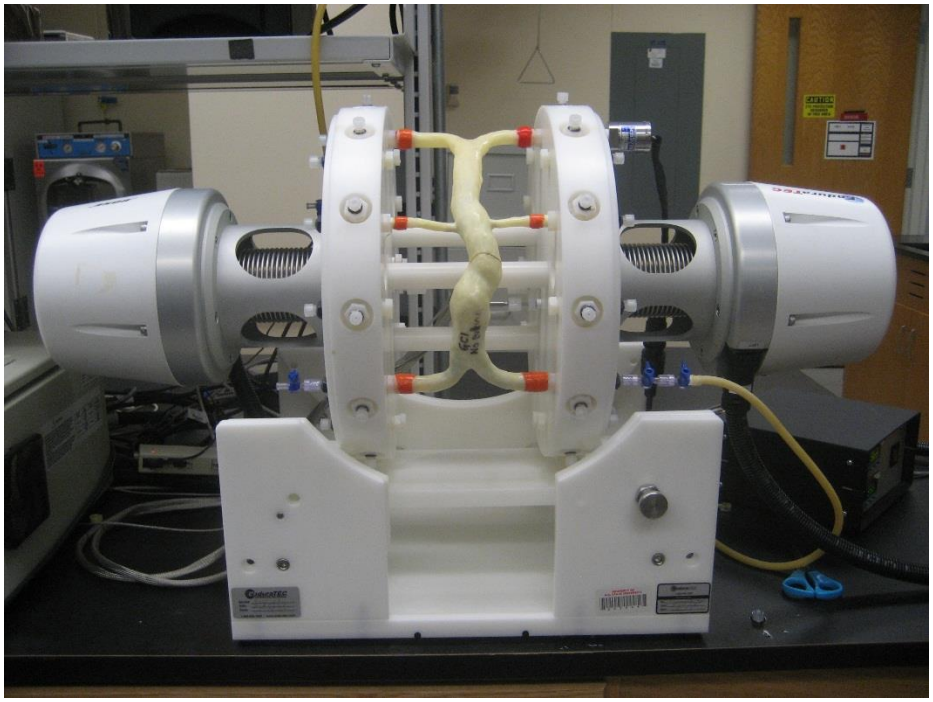

Figure 25: One of the devices (GC1) properly set up on the Bose Pulsatile Fatigue Tester

The pressure readings taken with the WinTest software that accompanies the Enduratec fatigue tester are said to be inaccurate at high frequencies, especially taking into account the unusual morphology of the device being tested. In order to assure that a hypertensive pressure was being achieved, a Keyence LS-5000 optical micrometer was used to measure the diameter. The diameter was taken while the machine was running at 1.2 Hz, or normal heart rate, and at a pressure of approximately 160/90 mmHg. Assuming that the distension would be the same at a higher frequency as long as the pressure would stay the same, the frequency was then increased to somewhere between 40 and 60 hertz (depending on the sample), and the water displacement was changed until the distension was approximately the same as it was at the

lower frequency. This displacement was then used for the rest of the test unless it became necessary to change it to keep the machine running.

In addition to checking the diameter for the initial setup, the diameter was checked regularly throughout the test to see if there was any increase. This was not intended to be a measure of the compliance of the stent grafts, but rather a measure of the compliance of the phantom material. As there was no thrombus included inside the lumen of the phantom, water was able to run not only through the lumen of the stent graft but also between the stent graft and the inner wall of the phantom, causing outward pressure. The change in diameter was monitored to see if the phantom was able to withstand this pressure. As the position of the stent graft was changed at every checkpoint, the diameter did not remain the same throughout the entire cycling. Therefore, only the change between the start at one checkpoint and end at the next checkpoint was considered.

As described before, the internal geometry of each phantom was slightly different, and each stent graft was different. Due to this, each device was tested with different settings on the Enduratec fatigue tester and will be outlined separately according to the order they were tested in. The order was randomized using Microsoft Excel. Any trends that can be seen in the pattern should be attributed to the small number of samples.

3.4.3.1 GC2

The displacement for this device was set at 1 mL for the high displacement and -1 mL for the low displacement, and a frequency of 50 Hz. There were no abnormalities during

testing, and the lumen of the stent graft was able to be visualized at all time points from both the proximal and distal end of the phantom.

3.4.3.2 GM2

The displacement for this device was set at 1 mL for the high displacement and 0 mL for the low displacement, and a frequency of 50 Hz. There were no unexpected shutdowns during the cycling of this device. The contralateral limb of the phantom had a tear in it that ran up from the edge to part of the way up the limb (See Figure 26). To be able to properly seal it, a small piece of copper tubing was inserted so that the silicone tape could be bound around the torn area and around the port without occluding the limb (See Figure 27).

Figure 26: The tear along the contralateral iliac artery of the GM2 phantom

Figure 27: The piece of copper tube inserted to allow silicone tape to be bound around the tear without occluding the limb.

3.4.3.3 GM1

During the cycling of this device the WinTest software experienced many shut downs due to overheating of the amplifier. It was initially set with a displacement of 5 mL over 0 mL and a frequency of 50 Hz. It ran for 15,000,000 cycles before it started having trouble. Several different frequencies and displacements were tried without success until it was run at 58 Hz and 1 mL/0 mL displacement. This device, similar to the previous one, also had tearing at the bottom two limbs which required the insertion of copper tubes. Imaging therefore could not be done from the bottom.

3.4.3.4 GC1

The displacement for this sample was initially set at 0.75 mL for the high displacement and 0 mL for the low displacement, and a frequency of 50 Hz. The high displacement was changed to 1 mL at approximately 410,000 cycles due to a drop in the maximum diameter, and the cycles were zeroed. However, after 100,000 cycles the diameter had again dropped slightly. It was suspected that this was a result of the phantom and stent graft relaxing, and could not be helped, so the tester was left running.

3.4.4 Imaging

An important concern during this testing was that the fenestration, due to being unsupported, might tear during the fatigue process. Images were therefore taken of the internal structure at the junctions of the graft material and the renal stent grafts at key time points. A high quality Olympus GIF XP160 Video Gastroscope 5.9mm in diameter was used to check for tears before the fatigue was started and after the 40,000,000 cycles were completed. This was completed under dry conditions at the North Carolina State University Veterinary Small Animal Clinic by Dr. Steve Marks.

In between these times the devices were internally inspected with a 6 mm borescope at key time points, those being 0 cycles, 1 million cycles, 5 million cycles, 15 million cycles, and 40 million cycles. To do these visualizations, the water was drained from the device and placed back into the tank, and one or more of both the distal and proximal branches was removed from the port so the lumen of the stent graft could be seen from the proximal and distal end. The branches were then reattached, the device refilled, and the test restarted

3.4.5 Macroscopic Evaluation

In order to determine whether any physical damage had been done to the stent grafts a macroscopic and microscopic evaluation were performed. For the macroscopic evaluation, the phantoms were carefully dissected and images were taken during the process to note the location of the limbs. The fenestration areas of the grafts were then carefully examined with the naked eye in a well-lit area and evaluated for defects, fraying, melting, and anything else that was notable.

3.4.6 Fenestration Measurement

The width and height of the fenestrations were measured both before and after removing the renal stent grafts. The measurement was done under an illuminated magnifying glass with digital Mitutoyo calipers. The renal stent grafts were removed by gently compressing them until they were able to fall through the fenestration without damaging the edge of the fenestration. All changes in the material were documented and photographed using a Canon digital camera.

3.4.7 Microscopic Evaluation

Standard optical microscopy could not be performed due to the size of the stent grafts and the focal distance required for most microscopes. Instead the evaluation was done using a Nikon SMZ1000 stereoscopic zoom microscope (See Figure 28). Each of the fenestration areas and holes was evaluated for fraying, polymer melting, change in fabric structure, tears, and

additional holes that could not be seen during the macroscopic evaluation. Images were taken using the microscope's software from 8x magnification to 80x magnification.

Figure 28: The Nikon stereoscope used to visualize the samples for the microscopic analysis [15].

3.4.8 Fabric Count

A fabric count was taken in order to see if the ballooning and subsequent pulsatile fatigue changed the spacing in the warp or weft fibers. It was expected that fatigue would cause the fibers in the unfenestrated fabric to space further apart.

The warp and weft count could not be taken using a traditional pick counter due to the tight weave of the fabric. Instead, high resolution images of the graft fabric were taken with flexible measuring tape held against it. The warp and weft count were taken over two millimeters, starting at a point approximately one millimeter away from the fenestration edge

(See Figure 29). The counts were taken above, below, and to the right and left of the fenestration. These measurements taken to the top, bottom, left, and right of both fenestrations were averaged to obtain a mean warp and weft value. The logic behind this was that the fenestrations performed on each side of the stent graft were done using the same conditions and fatigued under the same conditions. A warp and weft count were also taken on unfenestrated areas of the fatigued specimens, as well as on the control samples for comparison purposes.

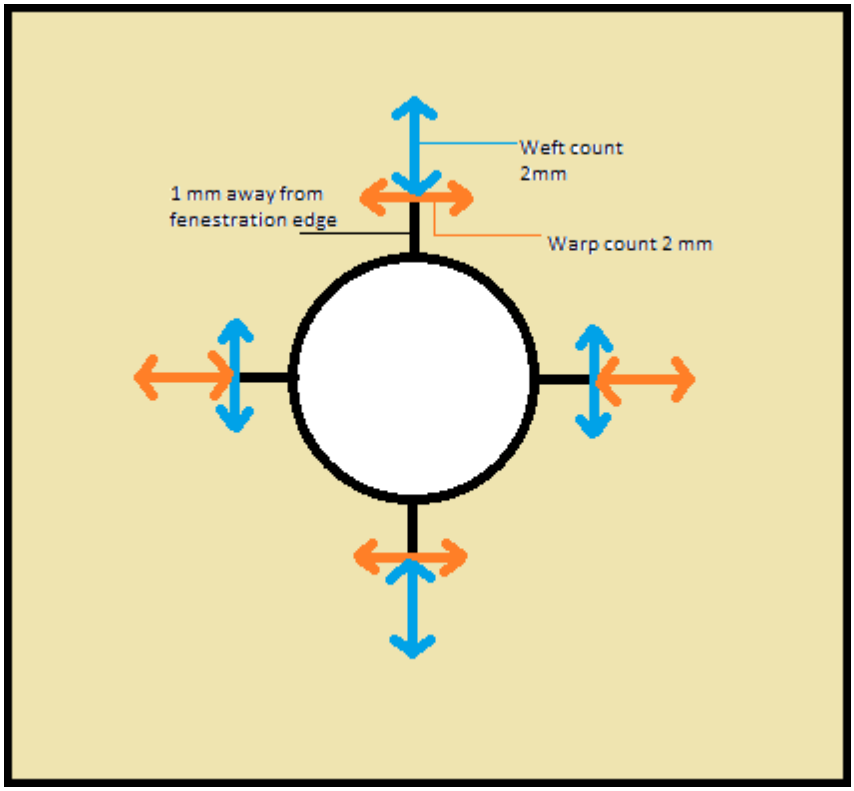

Figure 29: Showing the distance away from the fenestration where the weft and warp counts were made in each direction.

3.4.10 Probe Burst Resistance

The probe bursting resistance test was based off of the method used by Eadie [15]. It was performed in order to test the amount of force required to make a fenestration tear open. There was a concern that due to the fenestration being unsupported, it would not take much force to burst it open. The test is a smaller version of the ASTM D3787 Ball Burst Test Method, based off of the ISO test method for Cardiovascular Implants ISO 7198:1998 [61-62]. The cage used to clamp the fabric down is made of two separate parts. The bottom part, containing a clamp to hold the fabric in place, is what is controlled by the Instron tester. It is raised until the probe, held steady and attached to the top piece, is pierced through the fabric. The cage was attached to an Instron 5544 mechanical tester. The probe used had a diameter of 9.5 mm. The test speed was set to 100 mm/min. See Figure 30 for a view of the Probe Cage.

Figure 30: The probe burst cage used to test the burst resistance [15].

There was no clear way to use a probe to burst through a fenestration while the stent graft was still mostly intact, due to the cylindrical shape and the location of the fenestrations relative to the metal stents. Therefore, the decision was made to convert the graft fabric containing a fenestration into a flat sample. One fenestration per sample had to be chosen in order to fit on the tester. The fenestrations were chosen based off of location to extraneous holes. There was a concern that if a secondary hole was too close to the fenestration, the probe would cause them to tear open into one whole, causing inaccurate readings (See Figure 31). The metal stent rings that were closest to the fenestration were removed by carefully cutting the sutures using a sharpened razor blade. The fabric was then cut off from the rest of the graft

using scissors, and the resulting tube cut lengthwise halfway around the circumference from the chosen fenestration. The two control grafts similarly had the stents removed and the fabric cut.

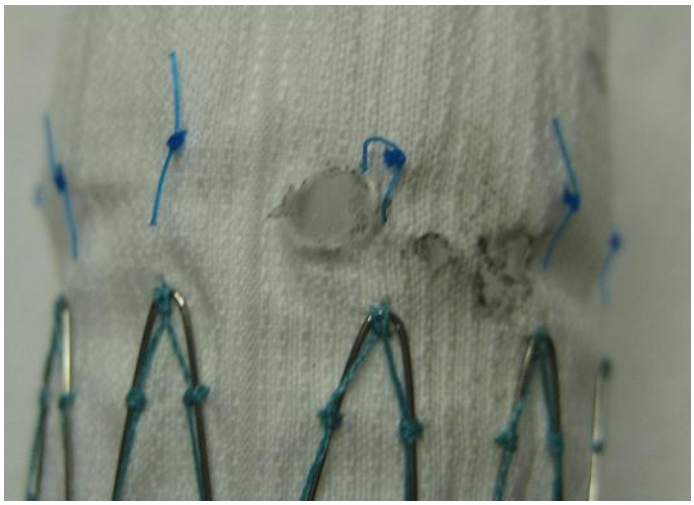

Figure 31: GC1 device with secondary holes close to the fenestration.

The chosen fenestrations were lined up with the probe, and the test started with the probe approximately 1 cm above the sample. The extension at break was also measured in order to see how much the fabric stretched before the fenestration tore open. The fenestrations chosen and their width and height are outlined in Table 4.

Table 4: The fenestrations chosen for the probe burst test and their measurements

Specimen	Fenestration	Width (mm)	Height (mm)
GC1	Left Renal	3.04	3.04
GC2	Right Renal	4.71	4.91
GM1	Left Renal	3.44	3.52
GM2	Left Renal	4.27	5.07

CHAPTER 4: RESULTS AND DISCUSSION

4.1 Results

This study was designed to be a demonstration of the changes to endovascular stent grafts that can be seen after fenestration and fatigue. Each of the devices had very unique results, so they will be outlined separately first, then the similarities and differences compared.

4.1.1 GC1

4.1.1.1 Macroscopic Analysis

A large hole could be seen to the right of the right renal fenestration. This hole could be seen during the initial look at the lumen of the stent graft using the high powered gastroscope, as well as during the subsequent viewings with the borescope. It was thought to have initially been multiple holes that were very close together and tore open to form one large hole. It was clearer that this was what happened during the microscopic analysis, as several threads could be seen that were still holding two parts of the hole apart (See Figure 32). A smaller hole was located beneath this one, not connected to it. Melted marks could be seen around the edges of both holes, as well as around the edges of the fenestration. The fenestration also contained evidence of fraying. Once the renal stents were removed a few long frayed fibers could be seen at the right renal fenestration site.

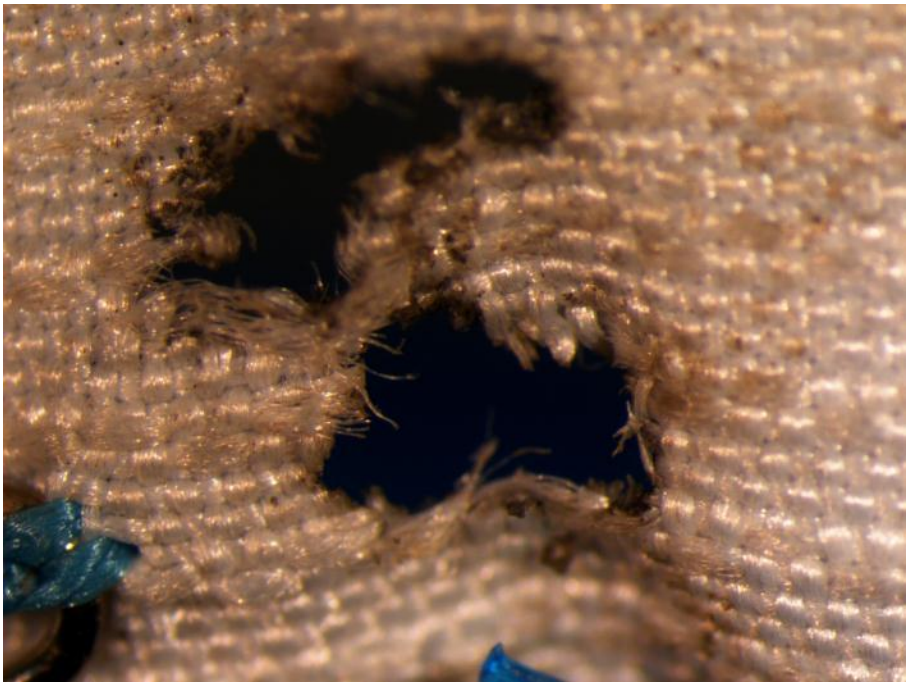

Figure 32: Microscopic view of largest secondary fenestration, 20x. Under macroscopic viewings it looked to be one hole; this image shows that it is two holes separated by a few threads.

The left renal fenestration also has a series of melted marks approximately five millimeters away from it. There were three distinct marks including one small hole less than one millimeter in diameter. Though these marks were not seen until the macroscopic analysis, they share similar characteristics with the fenestration holes, and so they likely were formed during the initial fenestration process. The left fenestration itself showed signs of melted marks and fraying, though there was more evidence of melting than fraying.

4.1.1.2 Fenestration Measurement

During the fenestration process it was noticed that the Cook fabric produced a waist even when ballooned up to 20 atm (See Figure 23). The uncut fenestrations continued to apply

pressure on the renal stent graft even after fatigue. Once the renal stents were removed, the fenestrations got smaller again as the fabric relaxed. The measurements can be seen in Table 5.

Table 5: The left and right renal fenestration dimensions before and after removing the renal extensions.

GC1	Before/After Removal	Width (mm)	Height (mm)
PR	Before	3.91	3.72
	After	3.14	3.11
PL	Before	3.87	3.94
	After	3.04	3.04

When the fabric was removed from the device for the probe burst test, it could be seen that the fenestration area had grown even smaller. This suggests that the fabric relaxed further over time.

4.1.1.3 Microscopic Analysis

Under high magnification melted and fused could more clearly be seen. For the right renal fenestration melted fibers could be seen around various parts of the circumference of the hole. All of the frayed fibers appeared to come from the warp direction, whereas the weft fibers seemed to be cut and melted (See Figure 33). It seems likely that the extra floats in the warp direction were pulled out as the fenestration was expanded due to the force of the balloon. The holes next to the right renal fenestration, which were not expanded, were melted around the entire circumference of the hold, and did not show evidence of fraying. The fraying seems to be caused by the ballooning. Near the fenestration area some fibers could be seen that appeared

to have been partially melted or melted, but were not fully cut through. This is interesting, as this was seen on the outside of the stent graft, which did not have direct contact with the RF puncture wire.

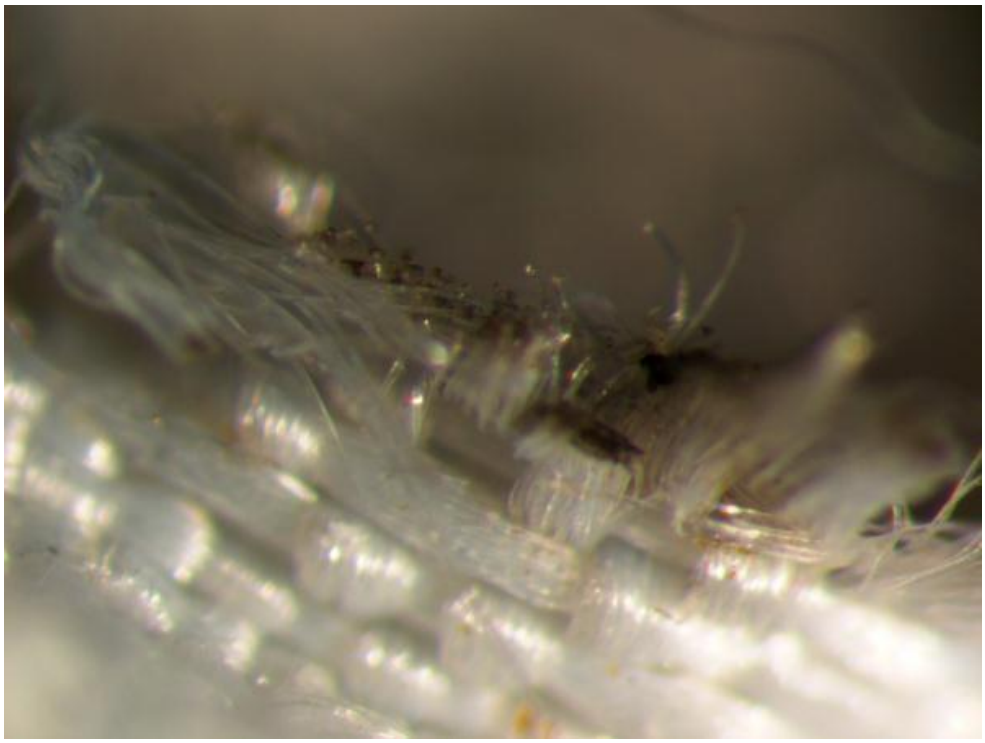

Figure 33: Melted and fused fibers at the edge of the right renal fenestration. It can be seen here that the weft yarns were cleanly melted, whereas the warp float was at least partially pulled out of the weave structure and frayed. 40x zoom.

The left renal fenestration had less damage overall than the right renal fenestration. There were not many melted fibers, though a piece of fabric was stuck at the top of the fenestration, probably pulled loose during the fenestration and subsequent ballooning. There was evidence again that most of the fraying was from the warp floats. The small hole near the

fenestration was similar to the small hole near the right renal fenestration, in that it was melted around the entire circumference with no evidence of fraying (See Figure 34).

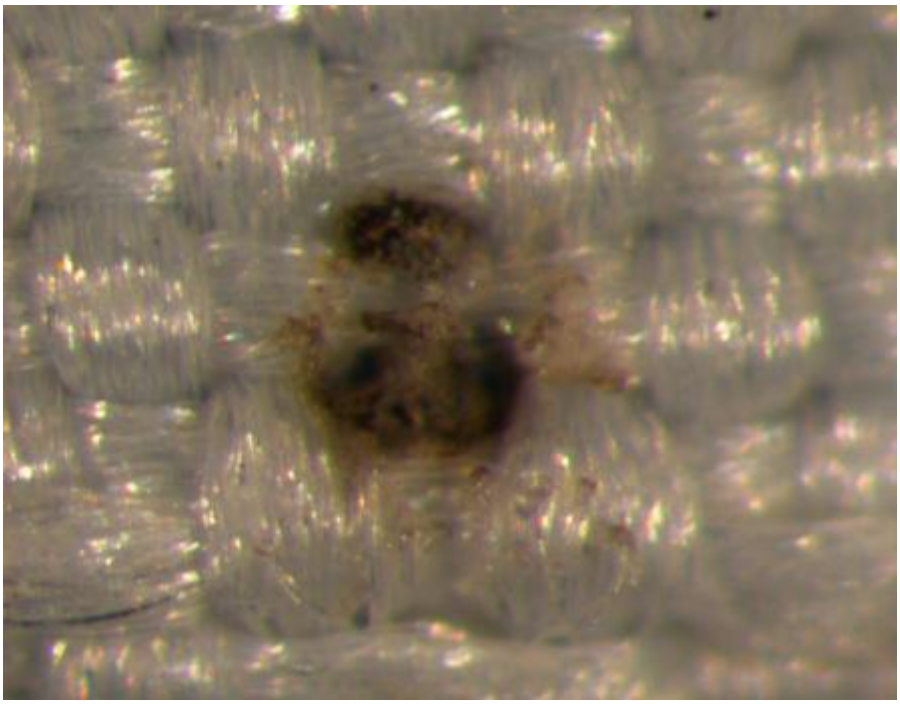

Figure 34: The smallest hole near the left renal fenestration. Due to the round nature and the discolored/melted fibers, it can be surmised that this resulted from an unsuccessful fenestration attempt. 80x zoom.

4.1.1.4 Fabric Count

Both the warp and the weft count varied at each point it was taken at. The results can be seen in Table 6. They are shown along with the measurements taken for the unfenestrated device for comparison.

Table 6: The warp and weft counts taken at each location on the GC1 device, and from the unfenestrated device.

Specimen	Warp (ends/cm)	Weft (picks/cm)
Cook Unfenestrated	90	114
GC1	105	116.25
GC1 Unfenestrated Area	80	115

On average both the warp and weft counts increased for the GC1 device, a more significant increase in the warp direction. The additional floats found in the warp direction did not prevent the fibers from ultimately moving closer together. The force created by the ballooning exceeded the resistance of the warp fibers. This does not compare with what Eadie found in her study. She did not find evidence that the ballooned fenestrations for the Cook fabric had a significantly different warp or weft count than the control specimen. However, her samples were tested under different conditions, and were not fatigued. The unfenestrated fatigued area on the GC1 device did have a significant drop in the warp count. This implies that the fatigue allowed for filament and yarn movement during the cycling on the non-fenestrated areas, causing the warp yarns to space further apart.

There was a small change seen in the weft count near the fenestrations but it did not seem to be a significant change, the difference being only 2.25 ends/cm compared to the control. Therefore, it can be surmised that the weft count did not change due to fenestrations. The unfenestrated area on the control device also did not have a significant change in weft count, so it can be concluded that neither fatigue nor fenestration with a standard angioplasty balloon affected the weft count.

4.1.1.5 Probe Burst Test

The probe burst test was performed on the left renal fenestration of the GC1 device, as it proved to be the larger fenestration when measured after removing the renal extension, and thus closest to the mean fenestration size for all devices. The stents were cut off and the tubular fabric cut so it would be flat and fit into the test used by Eadie [15]. The force required for the 9.5mm probe to burst through the fenestration, as well as the extension at the breaking point, can be seen in Table 7 as compared with the force required to break through the control device which had not been fatigued or fenestrated.

Table 7: The load and extension required to burst through the CU (Cook Unfenestrated) and GC1 devices

Specimen	Fenestration	Load at Break (N)	Extension at Break (mm)
CU	N/A	289.224	21.107
GC1	Left Renal	143.991	19.061

The force required to break through the unfenestrated device was much higher, nearly twice that of the fenestrated device. This is not surprising, as the fenestration provided a starting point for the probe. It was noted during the test that even with the fenestration the Cook fabric appeared to stretch quite far before bursting. No statistical analysis was performed due to the small number of samples. Eadie found much higher terminal loads when testing the Cook fabric; however, her samples were not fatigued, nor were they removed from a pre-fabricated stent graft. In order to achieve different diameters the stent graft fabric was likely heat set onto

different size mandrels. Therefore the warp and weft count would be different for each size stent graft, which would in turn affect the probe bursting strength. Both of these points explain why she saw different terminal loads than the ones experienced in this study.

4.1.2 GC2

4.1.2.1 Macroscopic Analysis

The Cook device fenestrated with the aid of a cutting balloon had no extraneous fenestration marks that were visible under the naked eye. The left renal artery fenestration had a healthy waist and did not visibly appear to reduce the diameter of the renal stent graft. There was clear evidence of fraying, more so than on the device that didn't use a cutting balloon. Once the renal extension was removed it could be seen that the fraying came from both the warp and weft yarns, but still primarily seemed to be from the warp floats. Melted fibers were also visible around the circumference of the fenestration.

The right renal artery fenestration also had no visible evidence of clamping down around the renal stent graft extension. Compared with the left renal fenestration, the fraying was less severe, and there were more melted marks. This indicates that the RF wire may have melted more yarns, preventing them from splitting apart and fraying when ballooned, and that the cutting balloon may not have scored as much of the fabric as on the other fenestration.

4.1.2.2 Fenestration Measurement

The fenestrations on this device were significantly larger than those on the non-cutting balloon device. The measurements of height and width were taken before and after removing

the renal extensions. The extensions were removed the same way as they were for the GC1 device. The measurements can be seen in Table 8.

Table 8: Fenestration Measurements before and after removing renal extensions.

GC2	Before/After Removal	Width (mm)	Height (mm)
PR	Before	4.89	5.31
	After	4.71	4.91
PL	Before	6.04	5.86
	After	3.96	4.66

The healthy waist mentioned earlier for both fenestrations is confirmed by the larger fenestration measurements as compared with the GC2 device. The cutting balloon, by scoring the fabric, likely cut through some of the melted and fused yarns allowing the fenestration to be expanded open to a larger area, and retain that area once the renal stent graft was deployed. The return to a smaller size after the extensions were removed is evidence of the high force that the Cook fabric exerted on the renal extension even with a cutting balloon.

4.1.2.3 Microscopic Analysis

The microscopic analysis confirmed conjectures created during the microscopic analysis. For the left renal artery fenestration there was more fraying than melted fibers as compared with the GC1 device, and the fraying did come from both the warp and weft directions. The higher magnification also confirmed that the weave structure was coming undone at the edges of the fenestration, likely due to the high pressure used to balloon it open.

The right renal artery seemed to be have more fused weft fibers. There were locations where it seemed that some of the warp yarns had either been pulled out of the structure or gone missing entirely. There was also evidence of a small section of raveling that was not visible under the naked eye. It is unknown when it originated due to the inability to visualize the graft fabric before fatigue. However, it may have been caused a cut from the cutting balloon. One edge of the tear was very neat, implying that it had been cut, not torn, and also implying that it did not propagate (See Figure 35).

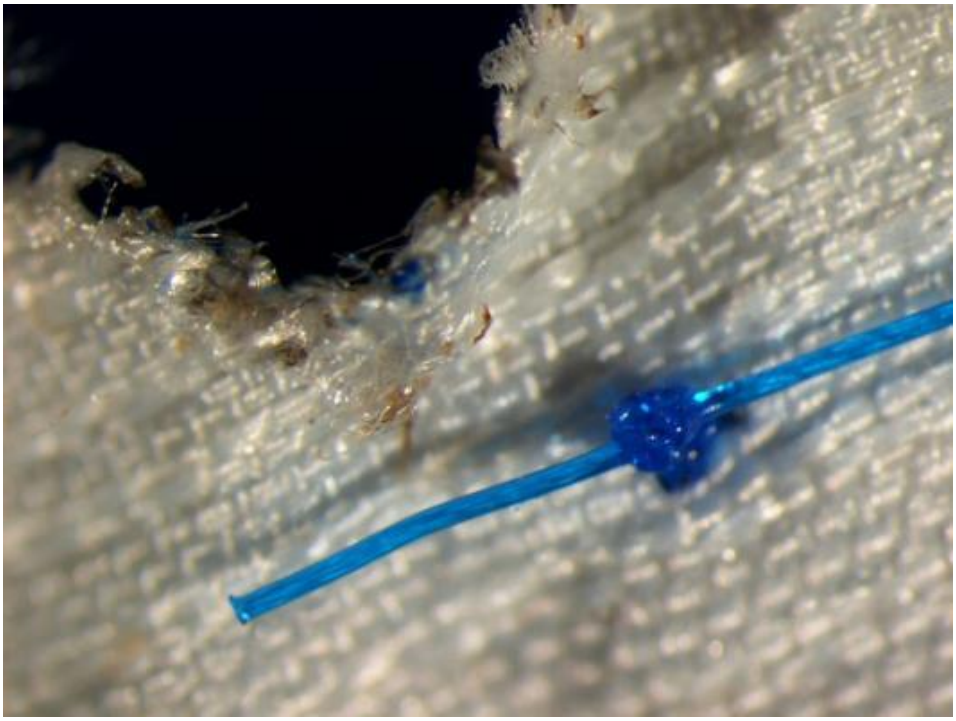

Figure 35: The raveled section as seen from the top at 20x zoom. Note the relatively clean edges.

4.1.2.4 Fabric Count

The GC2 device had the opposite warp and weft count changes than the GC1 device. The results can be seen in Table 9.

Table 9: Warp and Weft counts for the GC2 device and the control device

Specimen	Warp (ends/cm)	Weft (picks/cm)
Cook Unfenestrated	90	114
GC2	113.75	108.75
GC2 Unfenestrated Area	90	105

The average warp value for the area around the fenestration was higher than the warp counts for both the control device and the unfatigued area on the GC2 device. This shows that like the GC1 device the pressure caused by the balloon (in this case a cutting balloon) exceeded the motion resistance of the warp yarns, causing them to move closer together. The warp count for the unfenestrated area and the control device were the same. Though they were different on the GC1 device, the GC2 device had a different diameter which may have affected the warp count. This also applies to the weft count, which is lower in the case of the unfenestrated area of the GC2 device.

The average weft count was lower for the GC2 device around the fenestration area when compared to the control device. This implies that the use of a cutting balloon versus a standard angioplasty balloon lowers the weft count. However, it is still higher than the count for the unfenestrated area on the same device. Ergo, the ballooning still caused an increased

warp and weft count, and it is more likely that the fatigue testing caused the decrease in comparison to the control device.

4.1.2.6 Probe Burst Test

The right renal fenestration was chosen for the probe burst test as it was the larger of the two fenestrations. As with all of the other devices, only one fenestration could be used due to the small amount of fabric. The resulting force and extension required to burst through the fenestration can be seen in Table 10.

Table 10: The force and extension required to burst through the control fabric and the fenestrated fabric

Specimen	Fenestration	Load at Break (N)	Extension at Break (mm)
CU	N/A	289.22379	21.10663
GC2	Right Renal	51.04075	16.47664

The resulting force for the GC2 device is significantly lower than the force for the unfenestrated fabric. The larger hole likely made it easier for the probe to further tear the fabric. The extension was also smaller, suggesting that the fabric was strained less before breaking. The cutting balloon, having scored the fabric open and cut through some of the melted and fused fibers likely contributed to this force being so low. The existing tear may have also propagated, providing a starting point for the break.

4.1.3 GM1

4.1.3.1 Macroscopic Analysis

The macroscopic analysis of the Medtronic device fenestrated without the aid of the cutting balloon revealed similar behavior to the Cook devices. There was a single auxiliary holes that appears to have been caused by RF puncture, located approximately 2 mm away from the left renal fenestration. This hole was located right beneath the point of one of the metal stents, and measured 1.63 mm in height and 1.47 mm in width. Though it is fairly small, it is likely that the abrasion from the metal stent exacerbated its condition, causing the fraying, as no other auxiliary holes displayed any fraying. This hole was not seen during visualization using either the high powered gastroscope or the low powered borescope. The fabric component of the Medtronic graft has a tendency to form some wrinkles, and it is likely that a wrinkle covered this small hole while it was inside the phantom.

There was also evidence of fraying around both renal artery fenestrations. They did additionally show some evidence of fiber melting, but the fraying was more apparent. The left renal fenestration was ‘ideally’ positioned between metal stents on the bare fabric. The right renal fenestration was located at the bottom of a ‘V’ on the metal stent to which it was closest (See Figure 36). This location was not associated with any difficulties in ballooning, despite that the balloon would have been pushing against the stents. The fabric at the top end of the fenestration looked blackened, showing evidence of melted and melted fibers.

Figure 36: Showing the location of the right renal fenestration at the bottom of a 'V' stent

4.1.3.2 Fenestration Measurement

Both fenestrations shrunk in terms of height and width when the renal stent grafts were removed. The measurements can be seen in Table 11.

Table 11: Fenestration measurements of the GM1 device before and after renal graft removal

GM1	Before/After Removal	Width (mm)	Height (mm)
PR	Before	4.23	5.24
	After	3.69	4.08
PL	Before	4.85	4.68
	After	3.44	3.52

The measurements of the right renal artery may have been stunted by its location at the bottom of the ‘V’ of the metal stent. The height appears to be unaffected in comparison to the left renal artery, but the width is slightly smaller than the left renal artery fenestration. Both height and width shrunk for the two fenestrations, but not in a consistent manner. This can also be attributed to the location of the right renal fenestration.

4.1.3.3 Microscopic Analysis

Under macroscopic analysis the amount of fraying was much clearer, and was shown to be coming from both the warp and weft yarns. There was evidence of fiber melting (see Figure 37). The melting and fusing seemed to only occur at the very tips of the yarns. There were additionally some individual fibers that seemed to be melted at the tips. With the amount of fraying, it is likely that initially the entire yarns were melted, and the fibers from the yarns pulled apart due to the force created during ballooning.

Figure 37: Evidence of fraying at the edge of the fenestration, as well as some melted and fused fibers. 40x zoom.

The right renal fenestration had more fraying than the left renal fenestration, and under the high magnification it could be seen that the fenestration and fraying continued underneath the stent adjacent to the fenestration (see Figure 38). The fabric also buckled near the other side of the stent, due to not having the ability to expand any further (see Figure 39). At the top of the fenestration the weave structure had raveled slightly, not fully pulled apart but clearly more open.

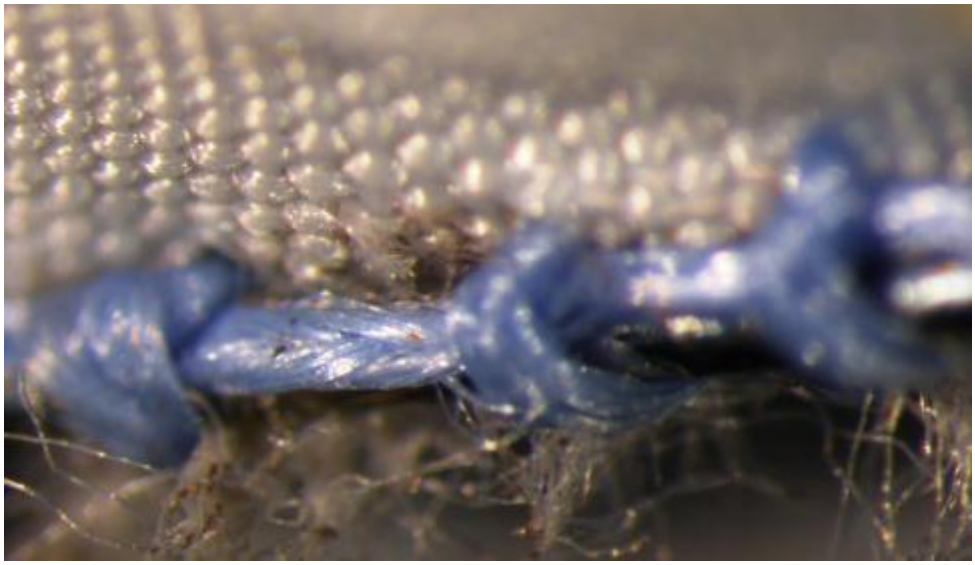

Figure 38: The fenestration and fraying continuing past the boundary of the metal stent. 40x zoom.

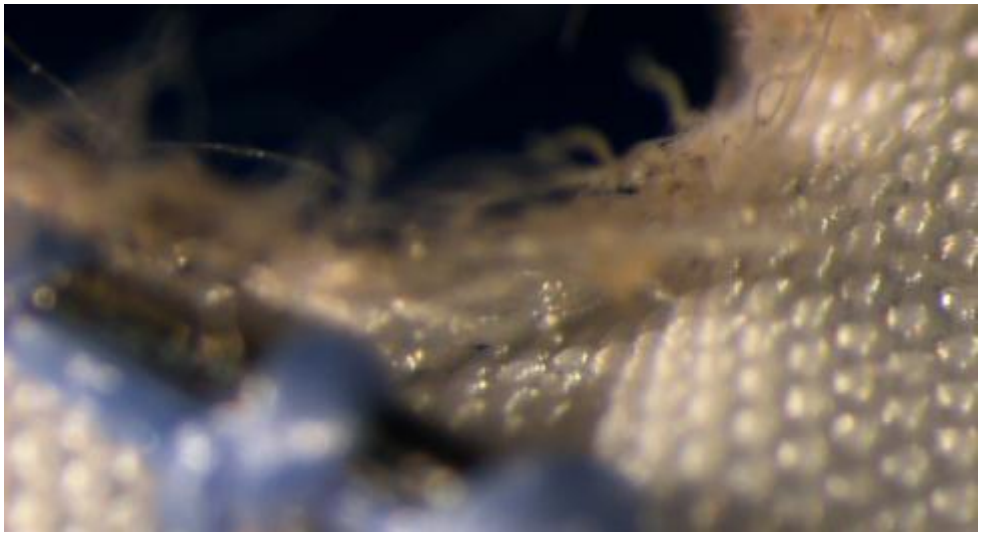

Figure 39: Fabric buckling as seen under 40x zoom

The small hole near the left renal fenestration showed more evidence that it was the result of an unsuccessful RF puncture. Melted fibers could be seen around nearly the entire

circumference of the hole (See Figure 40). The fraying, however, was also more apparent under microscopy, leading to the belief that its location under a stent caused some abrasion, aggravating the fibers. As this hole was not ballooned open, it is unlikely that the fraying on the renal fenestrations and the fraying on the hole had the same cause.

Figure 40: Hole underneath stent viewed from the top under 20x Zoom.

4.1.3.4 Fabric Count

The warp and weft counts for the GM1 were performed in the same manner as the previous samples. The results can be seen in Table 12. They are presented alongside the warp

and weft count for the Medtronic Endurant control device that was neither fatigued nor fenestrated.

Table 12: The warp and weft counts for the GM1 device and the Medtronic control device

Specimen	Warp (ends/cm)	Weft (picks/cm)
Medtronic Unfenestrated	106	118
GM1	129.29	126.43
GM1 Unfenestrated Area	105	115

The small difference between the unfenestrated GM1 fabric and the control fabric implies that fatigue did not have a significant effect on the warp and weft counts for the Medtronic fabric. Both the warp and the weft count averages around the fenestration edge, however, were much higher than both the unfenestrated GM1 area and the control device. This shows that the angioplasty ballooning caused the yarns in both directions to shift closer together in order to compensate for the force.

Eadie only found a significant difference in the amount of yarns in the warp direction between the standard fabric and the RF punctured and ballooned fabric. However, she did not take the warp and weft count of the fatigued fabric, and as mentioned for the GC1 device, the puncturing and ballooning were performed under different conditions.

4.1.3.6 Probe Burst Test

The probe burst test was performed on the left renal fenestration, as it was the larger of the two fenestrations and therefore closer in size to the smallest GM2 fenestrations (which were both larger than the largest GM1 fenestration). The results can be seen in Table 13.

Table 13: The load required to burst the GM1 fenestration and the unfenestrated control sample

Specimen	Fenestration	Load at Break (N)	Extension at Break (mm)
MU	N/A	138.99212	20.27788
GM1	Left Renal	70.87436	17.88643

The load and extension at break were both lower for the GM1 device than the unfenestrated control device. This was the expected result, as an existing fenestration eases the ability of the probe to burst through the fabric, causing both a lower ultimate load and lower strain.

Eadie had higher terminal loads when she tested RF punctured and ballooned fenestrations for their probe bursting resistance. Her devices were not subjected to fatigue resistance, and this is the most likely reason for the lower terminal loads in this study, as well as the different fenestration sizes.

4.1.4 GM2

4.1.4.1 Macroscopic Analysis

The left renal artery fenestration was at the top of one of the ‘M’ shaped stents on the metal stents. There was clear evidence of fraying around the fenestration. The frayed fibers seemed longer than on the GM1 device fenestrations. There were 2 possible small melted marks near the fenestration, but they could not clearly be visualized even under the illuminated microscope.

The right renal artery fenestration was bottom of a ‘V’ stent. It too showed a significant amount of fraying, the frayed fibers seeming longer in general than the GM1 fenestrations. There were a significant number of ‘melted’ marks close to the fenestration (though not interacting with it). There were five in total, including one hole and another possible hole. The clearly defined hole was very small, only 0.56 mm in width and 0.86 mm in height. It was melted around the edges. All of these marks were likely caused by unsuccessful attempts to puncture through the fabric.

4.1.4.2 Fenestration Measurement

Both of the renal artery fenestrations on the GM2 device managed to be ballooned to larger sizes as compared with the GM1 device. Even the fenestration located at the top part of an ‘M’ stent kept a large size. The measurements before and after removing the renal extensions can be seen in Table 14.

Table 14: Renal fenestration measurements for the GC2 device before and after removal of renal extensions

GM2	Before/After Removal	Width (mm)	Height (mm)
PR	Before	4.80	5.77
	After	4.40	5.17
PL	Before	5.42	6.23
	After	4.27	5.07

The left renal fenestration actually achieved values close to the diameter of the renal stent graft, which was 6 mm. Allowing for some compression in the cross direction, it seems that this fenestration was fully expanded and had no waist. This can be confirmed by the images taken under fluoroscopy, which also show no visible clamping around the renal fenestration (See Figure 41). In comparison, the GC1 fenestrations both had a small waist. This shows that the use of the cutting balloon allowed for the renal stent grafts to fully expand.

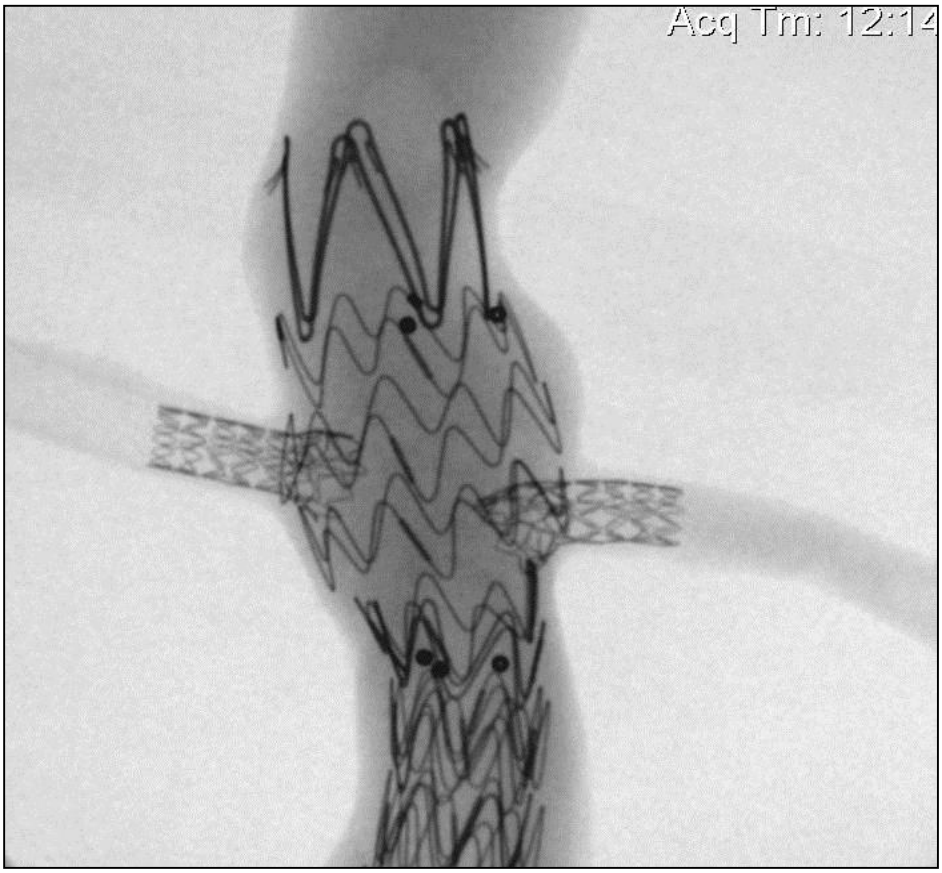

Figure 41: Fluoroscopic image of GC2 device showing both renal extensions without waist

Both renal fenestrations shrunk after the renal extensions were removed. The left renal extension shrunk the most, very likely due to the stent it was located under no longer being held open by the renal extension. The right renal fenestration did not shrink all that much in comparison. This could be due to the use of the cutting balloon during the fenestration process.

4.1.4.3 Microscopic Analysis

The microscopic analysis of the GM2 device revealed several features that were not seen during the macroscopic analysis. The right renal fenestration, located at the top of an ‘M’ stent, actually continues underneath the metal stent (See Figure 42). This was unexpected, as it was felt that the metal stents would prevent the fenestration from moving beyond its boundaries. The edges of the fenestration were mostly frayed fibers. The tips of the fibers were melted and melted, similar to those of the GM1 device, leading to the hypothesis that the RF puncture caused the yarns melt and fuse, and the subsequent ballooning pulled the fibers in those yarns apart. However, less fibers appear to have melted or discolored tips than in the GM1 device.

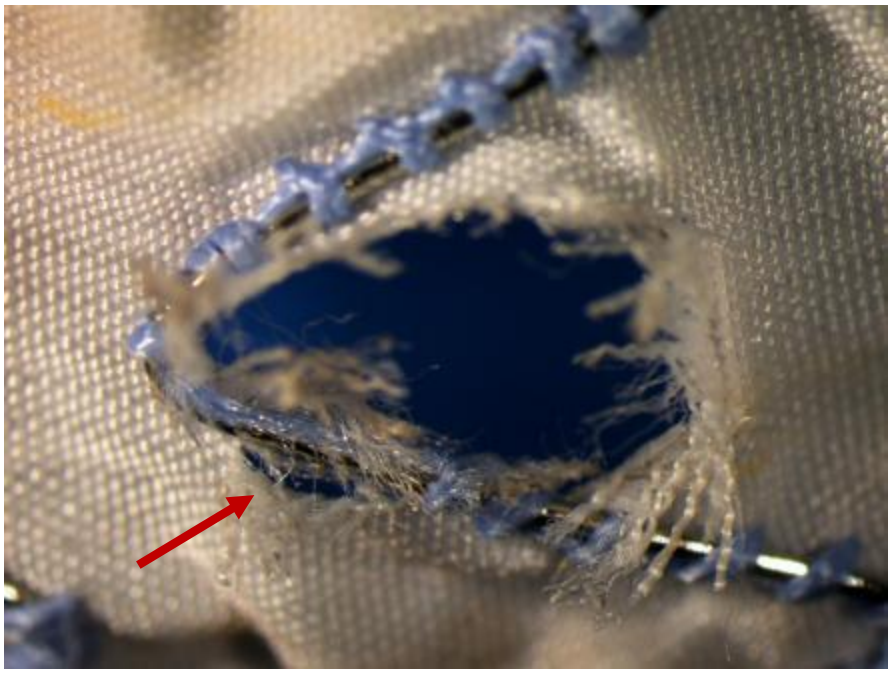

Figure 42: Right renal fenestration continuing under stent

The small hole near the right renal fenestration mostly showed melted and fused fibers (See Figure 43). The left renal fenestration showed slightly more intense fraying than the right renal fenestration. A small section of raveling could be seen on the right renal fenestration as well. It is not very clear due to the fraying in the area, but it is hypothesized that it was caused by the cutting balloon and the subsequent ballooning rather than the fatigue test. The fraying is not any more intense than in other sections, and appears more as though some of the fabric has come undone, rather than a tear (See Figure 44).

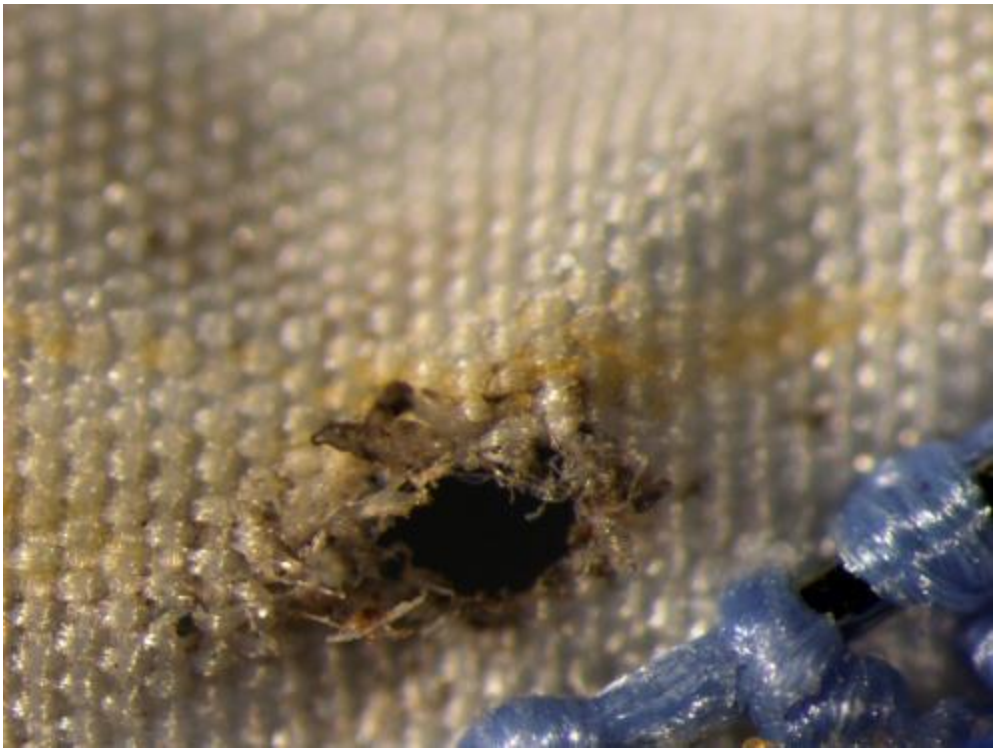

Figure 43: Small hole near right renal fenestration showing melted and fused fibers (10x Magnification).

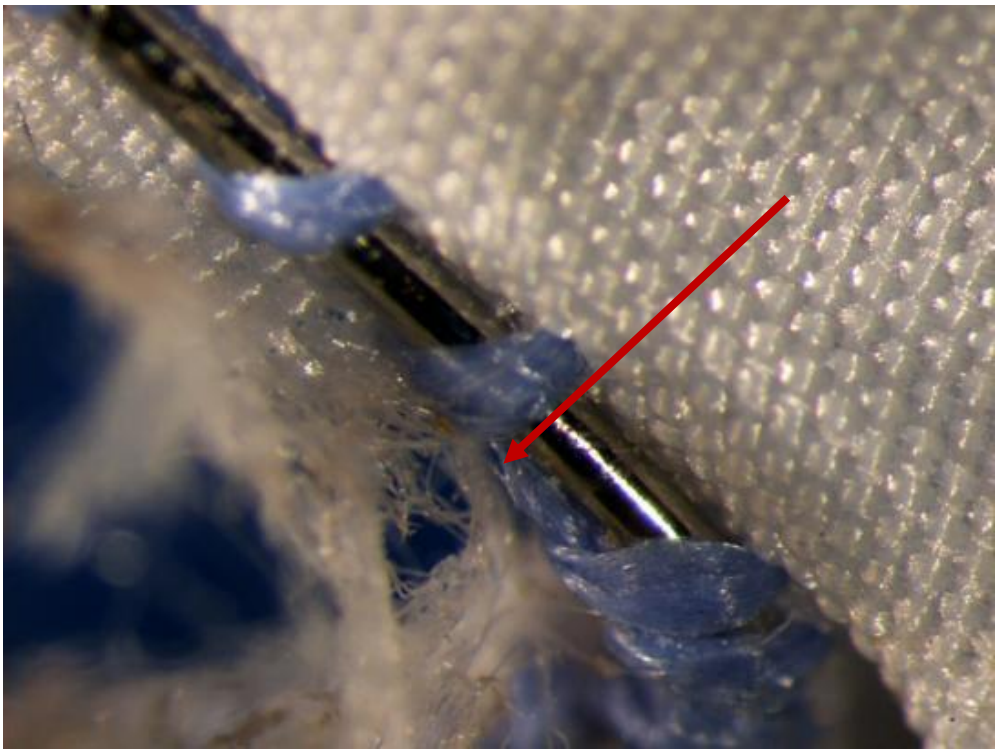

Figure 44: What could be a small raveled section on the GM2 device (30X magnification).

In addition to the fenestrations and the small hole noted earlier, there were also two very small holes near the left renal fenestration (See Figure 45). Under the highest magnification, there was evidence of melted fibers from the discoloration seen at the edges of the holes. Therefore it is likely that they too were caused by an unsuccessful RF puncture attempt. Though they could not be measured, the holes were not larger than the gaps created by the sutures in the fabric, so it is unlikely that if holes of this size occurred *in vivo*, a Type 3 endoleak would occur.

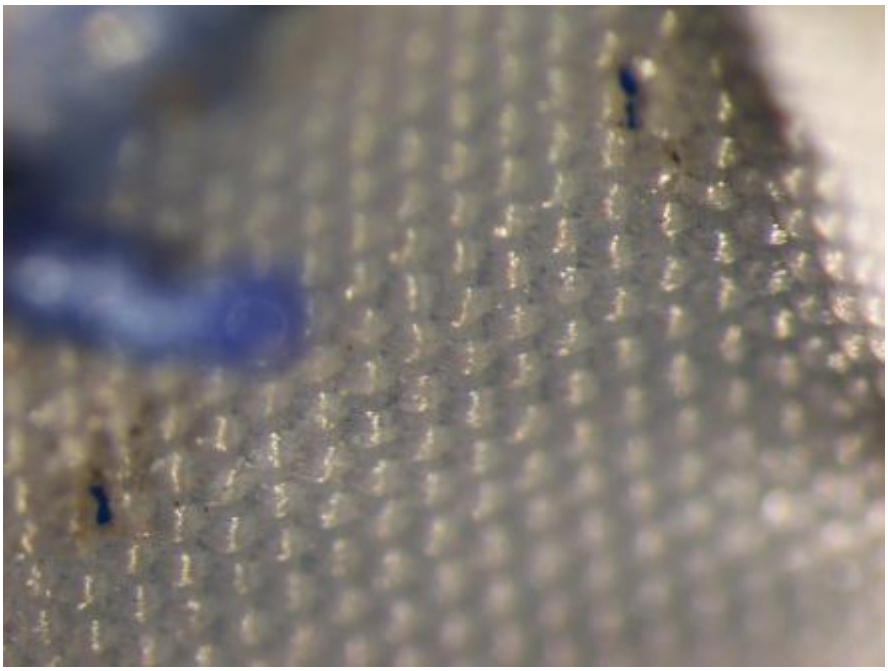

Figure 45: The two small holes located near the left renal fenestration. 40x zoom.

4.1.4.4 Fabric Count

Much like the GM1 device, the average warp and weft count for the fenestrated area of the GM2 device were higher than the control measurements. In this case, however, the warp count increased more than the weft count. The difference between the two samples can be attributed to the use of a cutting balloon versus a standard angioplasty balloon. The unfenestrated area on the fatigued device also had significantly higher warp and weft counts than the control device, compared to the GM1 device where there was a loss in ends and picks/cm on the GM1 unfenestrated area. Though an exact reason cannot be given for why this

happened, each device was unique and the fatigue testing, though standardized as much as possible, was not quite the same for each device. The results can be seen in Table 15.

Table 15: The fabric counts for the GM2 device and the Medtronic control device

Specimen	Warp (ends/cm)	Weft (picks/cm)
Medtronic Unfenestrated	106	118
GM2	114.375	120
GM2 Unfenestrated Area	115	125

4.1.4.6 Probe Burst Test

The amount of force required to 'break' open the left renal fenestration on the GM2 device was very low, slightly less than 1/16th of the force required to burst through the unfenestrated control sample. The force and extension can be seen in Table 16.

Table 16: The Load and Extension at Break for the Medtronic control device and the GM2 device.

Specimen	Fenestration	Load at Break (N)	Extension at Break (mm)
MU	N/A	138.992	20.278
GM2	Left Renal	8.521	15.833

Though the left renal fenestration was chosen because it was the smaller of the two fenestrations after the renal stents were removed, it was initially the larger fenestration. It can be surmised from this low load reading that although the graft fabric did relax into a smaller size, it did not regain its former strength.

4.2 Discussion

4.2.1 Fenestration process

Both types of stent graft, the Cook Zenith® and the Medtronic Endurant®, caused difficulties during the initial RF puncture of the fabric. The fabrics were resistant to the puncture, and the unsuccessful puncture attempts resulted in small holes as seen during both the macroscopic and microscopic analysis. The Cook fabric seemed to be more resistant to the puncture.

In comparing the effects of the use of RF and ballooning alone to RF and a cutting balloon, there is a significant difference in the size of the waist created on the renal stent graft, especially on the Cook fabric. It was most evident during the completion fluoroscopy. Figures compare the Medtronic stent grafts with and without the use of a cutting balloon. Though the waists are not very noticeable on the GM1 device, there is still a small amount of radial compression by the fenestration. In comparison, the GM2 device shows absolutely no evidence of a waist. Figures compare the Cook stent grafts with and without the use of a cutting balloon. The GC1 device shows two severe waists, which would not be ideal in a clinical setting. The narrowed opening to the renal artery would cause less blood to flow into the renal arteries, and possibly even thrombose closed entirely. Both events would have a very negative effect on the kidneys. On the other hand, both renal stent grafts show healthy waists on the GC2 device. The cutting balloon allowed the fenestration to be fully ballooned open. While there is still a small waist on the left (patient left) renal stent graft, it is a vast improvement over the GC1 fenestrations.

4.2.2 Macroscopic analysis

There were not many differences seen between the different samples for each type of stent graft that were not previously covered in the results. The GC1 device showed more melted and fused fibers around the edges of the fenestrations whereas the GC2 device showed more frayed fibers. The GM1 device and GM2 device both showed mostly frayed fibers around the fenestration edges, but both showed evidence of melted and fused fibers as well. The fraying seemed to increase for the devices fenestrated with the aid of a cutting balloon for both varieties of stent graft.

4.2.3 Microscopic Analysis

The microscopic analysis confirmed what was seen in the macroscopic analysis. The devices fenestrated with the aid of a cutting balloon showed a higher rate of fraying than those fenestrated without a cutting balloon. Evidence of melted or melted fibers could be seen on all samples, especially in the secondary (unintentional) holes.

4.2.4 Fenestration Measurement

The GC1 and GC2 devices had disparate measurements in both the height and width of the fenestrations, the measurements for the GC1 device being lower. As noted in Section 4.2.1, during fenestration the GC1 renal extensions exhibited a severe waist. Accordingly, the resulting fenestration measurements were smaller than those of the GC2, which did not have a severe waist formation for either fenestration. The GM1 and GM2 devices experienced the same disparate measurements, though the difference was not as severe between the two. The

cause was also the waist formed during fenestration without the aid of a cutting balloon. All of the fabrics relaxed and shrunk after the renal extensions were removed and radial pressure was no longer being applied. They were noticed to have shrunken additionally after several days, but no measurements were taken at the time. All results can be seen in Table 17.

Table 17: The fenestration heights and widths for each sample before and after removal of the renal stent grafts. PL=Patient Left, PR=Patient Right.

Specimen	Fenestration	Before/After Removal	Width (mm)	Height (mm)
GC1	PR	Before	3.91	3.72
		After	3.14	3.11
	PL	Before	3.87	3.94
		After	3.04	3.04
GC2	PR	Before	4.89	5.31
		After	4.71	4.91
	PL	Before	6.04	5.86
		After	3.96	4.66
GM1	PR	Before	4.23	5.24
		After	3.69	4.08
	PL	Before	4.85	4.68
		After	3.44	3.52
GM2	PR	Before	4.80	5.77
		After	4.40	5.17
	PL	Before	5.42	6.23
		After	4.27	5.07

4.2.5 Fabric Counts

The warp and weft counts were very dependent on the type of device as well as the fenestration technique. As a whole they were almost universally higher than the control devices, showing that ballooning (whether standard angioplasty or cutting) causes the yarns to

shift closer together in the area immediately surrounding the fenestration. It can be seen though that on both devices that used a cutting balloon, the weft count did not increase as much as when a standard angioplasty balloon was used. A possibility is that the cutting balloon placed more strain in the weft direction, causing the yarns to shift closer together. The results for all devices can be seen in Table 18. The measurements were not consistent with the findings by Eadie; however, she did not take fabric counts on fatigued specimens, and the testing conditions were radically different.

Table 18: Average warp and weft counts for all devices.

Specimen	Warp (ends/cm)	Weft (picks/cm)
Cook Unfenestrated	90	114
GC1	105	116.25
GC1 Unfenestrated Area	80	115
GC2	113.75	108.75
GC2 Unfenestrated Area	90	105
Medtronic Unfenestrated	106	118
GM1	129.29	126.43
GM1 Unfenestrated Area	105	115
GM2	114.375	120
GM2 Unfenestrated Area	115	125

4.2.7 Probe Bursting Test

The prediction for the probe bursting test results was that the unfenestrated devices would have the highest load at break, the fenestrated without a cutting balloon devices the second highest load at break, and the lowest would be the devices fenestrated with the aid of a cutting balloon. This prediction was seen in both the Cook devices and the Medtronic

devices. The fenestrations that did not use a cutting balloon were both smaller in size than their cutting balloon counterparts. This is what likely contributed to the difference in the load. The results can be seen in Table 19 and Figure 46.

Table 19: The Individual Results for each device showing the Load and Extension at Break

Specimen	Fenestration	Load at Break (N)	Extension at Break (mm)
CU	N/A	289.224	21.107
GC1	Left Renal	143.991	19.061
GC2	Right Renal	51.041	16.477
MU	N/A	138.992	20.278
GM1	Left Renal	70.874	17.886
GM2	Left Renal	8.521	15.833

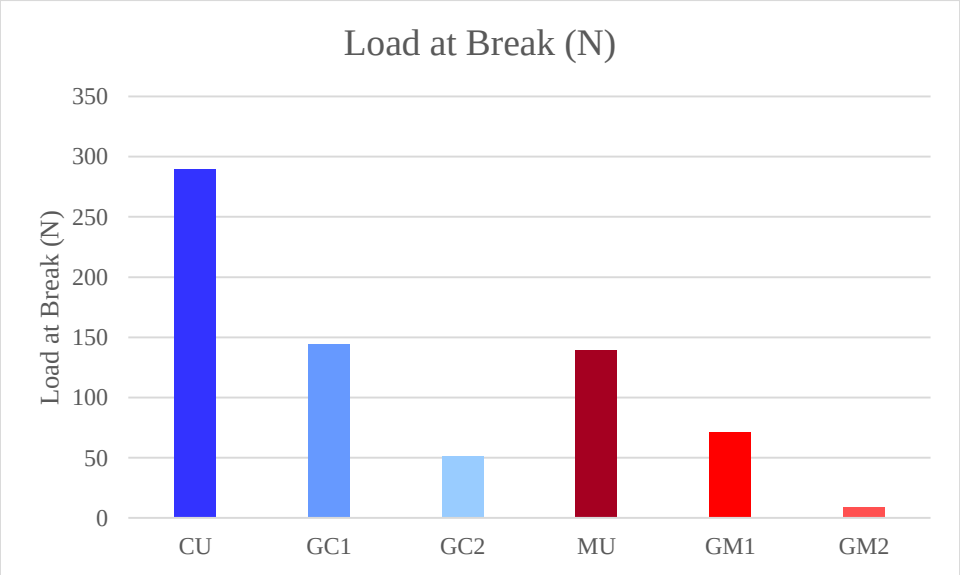

Figure 46: The load at break for each device during the probe burst test.

4.3 Extraneous holes

All but one of the devices (GC2) had one or more extraneous holes that were visible either under macroscopic or microscopic inspection. All of them showed signs of melted fibers around the entire circumference, and little evidence of fraying, suggesting that they were caused by unsuccessful attempts at fenestration with the RF puncture wire. It was noted during the fenestration process that it took several attempts to be able to successfully puncture through the fabric. Most of these holes were not able to be seen through endoscopic viewings. A list of the holes seen in the macroscopic analysis along with their measurements can be seen in Table 20.

Table 20: List of secondary fenestrations visible during macroscopic analysis plus dimensions

Device	Round (Y/N)	Height (mm)	Width (mm)	Comments
GC1	No	2.6	2.57	Two holes separated by threads
GC1	Yes	0.95	0.95	
GM1	No	1.63	1.47	Underneath stent
GM2	No	0.86	0.56	

The largest hole listed on the table was found on the GC1 device and had an abnormal shape. It was thought to be multiple holes very close together that formed into one larger hole, but during the microscopic analysis it was clear that the two major parts were separated by some threads, as seen in Figure 32. Each major part was still assumed to have been more than one hole initially, due to their abnormal shapes. This was the only hole that could be seen during endoscopic imaging.

The hole found on the GM1 device was likewise not round. However, it was located beneath a stent as seen in Figure 31. The fraying seen on it and the lack of roundness were likely caused by abrasion from the stent during pulsatile fatigue testing.

The other two holes listed on the table, as well as the holes seen during microscopic analysis, were small, and though they were not consistently round, they were consistently melted and fused around the edges and showed no signs of propagation. Had the holes propagated it would have been cause for concern, as it could have led to a Type III endoleak if presented in a patient. These small holes were likely not large enough to cause an endoleak *in vivo*; however, size of the defect does not directly correlate with the formation of an endoleak [23]. The two larger holes are concerning as they are close to 2 mm in both dimensions. Guidoin et al found upon studying explanted Stentor endografts that a defect 2 mm in diameter or larger was likely to form an endoleak rather than be covered by fibrin and thrombus [54].

CHAPTER 5: CONCLUSIONS

As outlined in Chapter One, the goal of this study was to determine and demonstrate the effect of *in situ* fenestration and the effects of two types of subsequent ballooning on the integrity of endovascular stent grafts by cycling them for the equivalent of one year *in vivo* on a pulsatile fatigue tester, and then evaluating the integrity using *in vitro* evaluation methods.

Overall there was no loss in integrity for any of the devices excluding the extraneous holes. Each of the devices behaved differently based on fabric type, stent type, and fenestration technique, but none of them lost their integrity. While the warp and weft count did decrease on certain samples, namely the GC1 in the unfenestrated area and the weft count of the GC2 in the unfenestrated area, the decrease was not enough to increase the porosity to the point of a Type IV endoleak.

The probe bursting resistance did decrease significantly with the GC2 and GM2 devices due to both the use of a cutting balloon and the larger fenestration size. However, this did not affect the overall integrity of the devices. The smallest force required to burst through a fenestration was still nearly ten times larger than what would be experienced *in vivo* [64]. In addition, though the fenestrations on the GC2 and GM2 devices were larger than on the GC1 and GM1 devices, the dimensions did not extend beyond the diameter of the Atrium® renal stent grafts, showing that the fenestrations did not increase in size due to fatigue.

A clinically relevant finding from this study was the appearance of extraneous holes on nearly all of the devices, save the GC2 device. As mentioned earlier these holes appeared to be the result of failed attempts to puncture through the graft fabric. Most of the holes were small, some even smaller than the holes formed from the sutures that anchored the stents to the

fabric, and it is likely that a layer of fibrin and thrombus would cover these holes and they would not form endoleaks [23]. However, two of the holes (one on GC1, one on GM1) were large enough that they exceeded or came close to the lower limit set by Guidoin et al for the size of hole that is likely to form an endoleak (2 mm diameter). Therefore, caution should be applied when using this puncture technique in order to ensure that no accidental Type III endoleaks are formed.

Specific Objectives

The specific objectives were to answer the following questions:

1. Are the warp and weft counts affected differently by use of a cutting balloon, and do they change after pulsatile fatigue?
2. Is the force required to burst the fabric with a probe different when a cutting balloon is used?
3. Are there any macroscopic or microscopic differences in the structure around the fenestration after fatigue between the normal RF puncture and the RF puncture with a cutting balloon? With the analysis done in the Results chapter all of these questions were able to be answered.

Question 1

The answer for this question is different for both the Medtronic devices and the Cook devices. The Cook devices both saw an increase in average warp count around the fenestration area compared to both the unfenestrated areas on the same devices and the control devices. The weft count for the GC2 device was lower than that for the control device but still higher than that for the unfenestrated area on the same GC2 device. The GC1 device showed a higher increase in weft count, whereas the GC2 device showed a higher increase in weft count, implying that the cutting balloon causes a difference in which direction the fibers move when pressure is applied. In terms of fatigue, the GC1 device had fewer ends/cm than the control device in the unfenestrated area, and the GC2 device had fewer picks/cm than the control device. The two stent grafts are different sizes, which may account for why they behaved differently in the unfenestrated areas.

Both the GM1 and GM2 devices had increased average warp and weft counts compared to the control device. The GM1 device experienced a much larger increase in ends/cm and picks/cm, implying that the standard angioplasty balloon causes a greater increase in fabric count, or at least creates a higher pressure on the surrounding fabric than a cutting balloon. Fatigue only seemed to affect the GM2 device. The GM1 unfenestrated area was not significantly different in terms of fabric count than the control device, but the GM2 device had an increase in both warp and weft. Though the devices were tested under similar standards, the nature of the pulsatile fatigue tests may have caused this difference between the two samples.

Question 2

The force required to burst the unfenestrated, unfatigued fabrics was the highest for both the Cook and the Medtronic devices. Without any initial tear to propagate through, it is unsurprising that these measured the highest. The force required for the fabric from the non-cutting balloon samples was approximately half that of the equivalent control fabric, for both the Cook and Medtronic fabrics. The addition of the cutting balloon made both of the fabrics much easier to burst. There are several possibilities that can explain why the force was so much smaller for the fenestrations that used the cutting balloon. The fenestrations were larger in width and weft when a cutting balloon was used. A larger hole makes it easier for the probe to burst. Another possibility, not mutually exclusive with the first, is that the melted and fused fibers, much more prevalent in the non-cutting balloon samples, made it more difficult to burst. Even so, the more likely of the two scenarios is that the smaller diameter caused the higher force readings.

Question 3:

Significant differences were noticed between the RF punctured samples and the RF punctured samples that also used a cutting balloon in terms of the fiber and fabric morphology around the fenestration area. For the Cook devices it was clear that there was a lot more fraying of the fibers around the fenestration edge when a cutting balloon was used, and there was less evidence of melted and fused fibers, likely because they had been pulled apart. On the GC1 device, which did not use a cutting balloon, both fenestrations only showed fraying of the warp floats that had been pulled out of the weave structure, whereas

the cutting-balloon device also showed fraying in the warp direction. There were also sections where the fabric raveled on the cutting-balloon device for both Medtronic and Cook. The Medtronic devices showed fraying in both directions for the fenestrations that didn't use a cutting balloon, but there was still some evidence of fibers that had been discolored and melted from the RF puncture. The GM2 device, which used the cutting balloon, showed significantly more fraying, and it was more difficult to find evidence of melted fibers.

Future Work

The results from this demonstration study were promising, but more data needs to be collected before making too many assumptions about the efficacy of this technique. Recommendations for future work are as follows:

1. A larger sample size would allow for statistical analysis to be performed and show if the results obtained here were sound.
2. Increasing the length of the fatigue analysis to 400,000,000 cycles would give the data at the equivalent of ten years *in vivo*. Combined with an increased sample size, it could be tested whether or not there is a correlation between the measurements and observations and the time *in vivo*.
3. Better endoscopic technology would allow for holes or tears formed before or during the fatigue to be monitored and measured to make sure they are not propagating, which would likely lead to a Type III endoleak.

REFERENCES

1. *Abdominal aortic aneurysm: MedlinePlus medical encyclopedia* Retrieved 3/23/2013, 2013, from http://www.nlm.nih.gov/medlineplus/ency/article/000162.htm
2. *CDC - DHDSP - fact sheets - aortic aneurysm fact sheet* Retrieved 3/6/2013, 2013, from http://www.cdc.gov/dhdsp/data_statistics/fact_sheets/fs_aortic_aneurysm.htm
3. Watson, C. J. E., Walton, J., Shaw, E., Heather, B., & Collin, J. (1997). What is the long-term outcome for patients with very small abdominal aortic aneurysms? *European Journal of Vascular and Endovascular Surgery*, *14*(4), 299-304. doi:10.1016/S1078-5884(97)80242-0
4. WRITING GROUP MEMBERS, Lloyd-Jones, D., Adams, R. J., Brown, T. M., Carnethon, M., Dai, S., et al. (2010). Heart disease and stroke Statistics—2010 update. *Circulation*, *121*(7), e46-e215. doi:10.1161/CIRCULATIONAHA.109.192667
5. *Abdominal aortic aneurysm: Treatments and drugs - MayoClinic.com* Retrieved 3/24/2013, 2013, from http://www.mayoclinic.com/health/abdominal-aortic-aneurysm/DS01194/DSECTION=treatments-and-drugs
6. Parodi JC, Palmaz JC, Barone HD. Transfemoral intraluminal graft implantation abdominal aortic aneurysms. Ann Vasc Surg 1991;5:491-9.
7. Kahn RA, Moskowitz DM. Endovascular aortic repair. J Cardiothorac Vasc Anesth 2002 4;16(2):218-33.

8. *Zenith flex(R) AAA endovascular graft with the Z-trak(TM) introduction system instructions for use*. Bloomington, Indiana: Cook Medical.
9. Oderich, G. S., Fatima, J., & Gloviczki, P. (2011). Stent graft modification with mini-cuff reinforced fenestrations for urgent repair of thoracoabdominal aortic aneurysms. *Journal of Vascular Surgery*, *54*(5), 1522-1526. doi:10.1016/j.jvs.2011.06.023; 10.1016/j.jvs.2011.06.023
10. Ricotta, J. J.,2nd, & Oderich, G. S. (2008). Fenestrated and branched stent grafts. *Perspectives in Vascular Surgery and Endovascular Therapy*, *20*(2), 174-87; discussion 188-9. doi:10.1177/1531003508320491; 10.1177/1531003508320491
11. Chuter, T. A. (2007). Fenestrated and branched stent-grafts for thoracoabdominal, pararenal and juxtarenal aortic aneurysm repair. *Seminars in Vascular Surgery*, *20*(2), 90-96. doi:10.1053/j.semvascsurg.2007.04.006
12. Greenberg, R. K., Sternbergh III, W. C., Makaroun, M., Ohki, T., Chuter, T., Bharadwaj, P., et al. (2009). Intermediate results of a united states multicenter trial of fenestrated endograft repair for juxtarenal abdominal aortic aneurysms. *Journal of Vascular Surgery*, *50*(4), 730-737.e1. doi:10.1016/j.jvs.2009.05.051
13. Tse, L. W., Steinmetz, O. K., Abraham, C. Z., Valenti, D. A., Mackenzie, K. S., Obrand, D. I., et al. (2004). Branched endovascular stent-graft for suprarenal aortic aneurysm: The future of aortic stent-grafting? *Canadian Journal of Surgery.Journal Canadien De Chirurgie*, *47*(4), 257-262.
14. Tse, L. W. H., Bui, B. T., Lerouge, S., Salazkin, I., Therasse, E., Benko, A., et al. (2007). In vivo antegrade fenestration of abdominal aortic stent-grafts. *Journal of*

Endovascular Therapy, *14*(2), 158-167. doi:10.1583/1545-1550(2007)14[158:IVAFOA]2.0.CO;2

15. Eadie, L. A. (2010). *The investigation of the effect of in situ radiofrequency fenestration on the textile components of endovascular stent grafts.* Unpublished Master of Science, North Carolina State University, NCSU Institutional Repository.
16. *Abdominal aortic aneurysm. JPEG image.* Retrieved 3/11, 2013, from http://www.ncbi.nlm.nih.gov/pubmedhealth/PMH0001233/bin/18072.jpg
17. Johnsen, S. H., Forsdahl, S. H., Singh, K., & Jacobsen, B. K. (2010). Atherosclerosis in abdominal aortic aneurysms: A causal event or a process running in parallel? the tromso study. *Arteriosclerosis, Thrombosis, and Vascular Biology*, *30*(6), 1263-1268. doi:10.1161/ATVBAHA.110.203588; 10.1161/ATVBAHA.110.203588
18. *ESC | communities | ESC councils | council for cardiology practice | E-journal of cardiology practice | inflammatory aortic aneurysm* Retrieved 3/11/2013, 2013, from http://www.escardio.org/communities/councils/ccp/e-journal/volume7/Pages/inflammatory-aortic-aneurysm.aspx#.UT1buFc2fWV
19. Hellmann DB, Grand DJ,Freischlag JA. (2007). INflammatory abdominal aortic aneurysm. *Jama*, *297*(4), 395-400. doi:10.1001/jama.297.4.395
20. Haug, E. S., Skomsvoll, J. F., Jacobsen, G., Halvorsen, T. B., Saether, O. D., & Myhre, H. O. (2003). Inflammatory aortic aneurysm is associated with increased incidence of autoimmune disease *Journal of Vascular Surgery*, *38*(3), 492-497.
21. *Inflammatory aortic aneurysm (JPEG image, 1800 × 1138 pixels) - scaled (49%).* Retrieved 3/24/2013, 2013, from

http://img.medscape.com/pi/emed/ckb/emergency_medicine/756148-756734-756735-1979845.jpg

22. *Types of aortic aneurysms, heart and vascular care, UW health, university of wisconsin hospital, madison , UW health, university of wisconsin hospital, madison* Retrieved 3/11/2013, 2013, from http://www.uwhealth.org/heart-cardiovascular/types-of-aortic-aneurysms/10973
23. *Personal communications with Dr. Leonard Tse*(2012-2013). In Ruthrauff A. (Ed.),
24. *Abdominal aortic aneurysm - stanford vascular & endovascular care - stanford hospital & clinics - stanford medicine* Retrieved 3/23/2013, 2013, from http://stanfordhospital.org/clinicsmedServices/COE/surgicalServices/vascularSurgery/patientEducation/abdomin.html
25. Maton, Anthea; Roshan L. Jean Hopkins, Charles William McLaughlin, Susan Johnson, Maryanna Quon Warner, David LaHart, Jill D. Wright (1993). Human Biology and Health. Englewood Cliffs, NJ: Prentice Hall. ISBN 0-13-981176-1. OCLC 32308337.
26. Peterson, B. G., Matsumura, J. S., Brewster, D. C., Makaroun, M. S., & Excluder Bifurcated Endoprosthesis Investigators. (2007). Five-year report of a multicenter controlled clinical trial of open versus endovascular treatment of abdominal aortic aneurysms. *Journal of Vascular Surgery*,*45*(5), 885-890. doi:10.1016/j.jvs.2007.01.044
27. Nedeau, A. E., Pomposelli, F. B., Hamdan, A. D., Wyers, M. C., Hsu, R., Sachs, T., et al. (2012). Endovascular vs open repair for ruptured abdominal aortic

aneurysm. *Journal of Vascular Surgery, 56*(1), 15-20. doi:10.1016/j.jvs.2011.12.067; 10.1016/j.jvs.2011.12.067

28. Paravastu, S. C., Ghosh, J., Murray, D., Farquharson, F. G., Serracino-Inglott, F., & Walker, M. G. (2009). A systematic review of open versus endovascular repair of inflammatory abdominal aortic aneurysms. *European Journal of Vascular and Endovascular Surgery : The Official Journal of the European Society for Vascular Surgery, 38*(3), 291-297. doi:10.1016/j.ejvs.2009.05.005; 10.1016/j.ejvs.2009.05.005
29. Saqib, N., Park, S. C., Park, T., Rhee, R. Y., Chaer, R. A., Makaroun, M. S., et al. (2012). Endovascular repair of ruptured abdominal aortic aneurysm does not confer survival benefits over open repair. *Journal of Vascular Surgery, 56*(3), 614-619. doi:10.1016/j.jvs.2012.01.081; 10.1016/j.jvs.2012.01.081
30. Veith, F. J., Baum, R. A., Ohki, T., Amor, M., Adiseshiah, M., Blankensteijn, J. D., et al. (2002). Nature and significance of endoleaks and endotension: Summary of opinions expressed at an international conference *Journal of Vascular Surgery, 35*(5), 1029-1035.
31. Heikkinen, M. A., Arko, F. R., & Zarins, C. K. (2004). What is the significance of endoleaks and endotension *The Surgical Clinics of North America, 84*(5), 1337-52, vii. doi:10.1016/j.suc.2004.04.009
32. White, S. B., & Stavropoulos, S. W. (2009). Management of endoleaks following endovascular aneurysm repair *Seminars in Interventional Radiology, 26*(1), 33-38. doi:10.1055/s-0029-1208381; 10.1055/s-0029-1208381

33. Tzortzis, E., Hinchliffe, R. J., & Hopkinson, B. R. (2003). Adjunctive procedures for the treatment of proximal type I endoleak: The role of peri-aortic ligatures and palmaz stenting *Journal of Endovascular Therapy : An Official Journal of the International Society of Endovascular Specialists, 10*(2), 233-239. doi:2
34. Baum, R. A., Carpenter, J. P., Golden, M. A., Velazquez, O. C., Clark, T. W., Stavropoulos, S. W., et al. (2002). Treatment of type 2 endoleaks after endovascular repair of abdominal aortic aneurysms: Comparison of transarterial and translumbar techniques *Journal of Vascular Surgery, 35*(1), 23-29.
35. Robert E O'Connor, MD, MPH. (2011). *Emergent management of abdominal aortic aneurysm rupture* Retrieved 3/6/2013, 2013, from http://emedicine.medscape.com/article/756735-overview#aw2aab6b3
36. *Recently-approved devices > endurant stent graft system - P100021* Retrieved 3/7/2013, 2013, from http://www.fda.gov/MedicalDevices/ProductsandMedicalProcedures/DeviceApprovalsandClearances/Recently-ApprovedDevices/ucm240094.htm
37. *Medtronic endurant inside an AAA (JPEG image, 311 × 524 pixels).* Retrieved 3/24/2013, 2013, from http://cdn.medgadget.com/img/5ked56h.jpg
38. *The endurant stent graft system IFU*. Minneapolis, Minnesota: Medtronic.
39. Makaroun, M. S., Tuchek, M., Massop, D., Henretta, J., Rhee, R., Buckley, C., et al. (2011). One year outcomes of the united states regulatory trial of the endurant stent graft system. *Journal of Vascular Surgery, 54*(3), 601-608.e1. doi:10.1016/j.jvs.2011.03.002

40. Setacci, F., Sirignano, P., de Donato, G., Chisci, E., Iacoponi, F., Galzerano, G., et al. (2012). AAA with a challenging neck: Early outcomes using the endurant stent-graft system. *European Journal of Vascular and Endovascular Surgery, 44*(3), 274-279. doi:10.1016/j.ejvs.2012.04.031

41. Torsello, G., Troisi, N., Donas, K. P., & Austermann, M. (2011). Evaluation of the endurant stent graft under instructions for use vs off-label conditions for endovascular aortic aneurysm repair. *Journal of Vascular Surgery, 54*(2), 300-306. doi:10.1016/j.jvs.2010.12.062

42. *Recently-approved devices > zenith® AAA endovascular graft - P020018* Retrieved 3/8/2013, 2013, from http://www.fda.gov/MedicalDevices/ProductsandMedicalProcedures/DeviceApprovalsandClearances/Recently-ApprovedDevices/ucm082436.htm

43. *Zenith flex(R) AAA endovascular graft with the Z-trak(TM) introduction system instructions for use*. Bloomington, Indiana: Cook Medical*Cook medical | aortic intervention* Retrieved 3/24/2013, 2013, from http://www.cookmedical.com/ai/home.do

44. Bos, W. T. G. J., Tielliu, I. F. J., Zeebregts, C. J., Prins, T. R., van den Dungen, J. J. A. M., & Verhoeven, E. L. G. (2008). Results of endovascular abdominal aortic aneurysm repair with the zenith stent-graft. *European Journal of Vascular and Endovascular Surgery, 36*(6), 653-660. doi:10.1016/j.ejvs.2008.07.010

45. Mertens, J., Houthoofd, S., Daenens, K., Fourneau, I., Maleux, G., Lerut, P., et al. (2011). Long-term results after endovascular abdominal aortic aneurysm repair using

the cook zenith endograft. *Journal of Vascular Surgery, 54*(1), 48-57.e2. doi:10.1016/j.jvs.2010.12.068

46. *Recently-approved devices > zenith® fenestrated AAA endovascular graft (with the adjunctive zenith alignment stent) - P020018/S040* Retrieved 3/24/2013, 2013, from http://www.fda.gov/MedicalDevices/ProductsandMedicalProcedures/DeviceApprovalsandClearances/Recently-ApprovedDevices/ucm300704.htm
47. Halak, M., Goodman, M. A., & Baker, S. R. (2006). The fate of target visceral vessels after fenestrated endovascular aortic Repair—General considerations and mid-term results. *European Journal of Vascular and Endovascular Surgery, 32*(2), 124-128. doi:10.1016/j.ejvs.2006.01.012
48. *IFU-FU - zenith fenestrated AAA endovascular graft - US.pdf* Retrieved 3/11/2013, 2013, from http://www.cookmedical.com/zenith/fenestrated/resources/IFU-FU - Zenith Fenestrated AAA Endovascular Graft - US.pdf
49. Correa, M. P., & Oderich, G. S. (2012). Percutaneous endovascular repair of juxtarenal aortic aneurysm using customized cook zenith fenestrated stent graft. *Journal of Vascular Surgery, 56*(6), 1827. doi:10.1016/j.jvs.2012.10.049
50. Verhoeven, E. L. G., Vourliotakis, G., Bos, W. T. G. J., Tielliu, I. F. J., Zeebregts, C. J., Prins, T. R., et al. (2010). Fenestrated stent grafting for short-necked and juxtarenal abdominal aortic aneurysm: An 8-year single-centre experience. *European Journal of Vascular and Endovascular Surgery, 39*(5), 529-536. doi:10.1016/j.ejvs.2010.01.004

51. Ricco, J. -. (2010). Fenestrated stent grafting for aortic aneurysm in europe. *European Journal of Vascular and Endovascular Surgery, 39*(5), 545-546. doi:10.1016/j.ejvs.2010.01.014

52. Amiot, S., Haulon, S., Becquemin, J. -., Magnan, P. -., Lermusiaux, P., Goueffic, Y., et al. (2010). Fenestrated endovascular grafting: The french multicentre experience. *European Journal of Vascular and Endovascular Surgery, 39*(5), 537-544. doi:10.1016/j.ejvs.2009.12.008

53. King, M. W., Zhang, Z., & Guidoin, R. (2001). Microstructural changes in polyester biotextiles during implantation in humans. *Journal of Textile and Apparel, Technology and Management, 1*(3), 1-8.

54. Guidoin, R., Marois, Y., Douville, Y., King, M. W., Castonguay, M., TraorÃ©, A., et al. (2000). First-generation aortic endografts: Analysis of explanted stentor devices from the EUROSTAR registry. *Journal of Endovascular Therapy, 7*(2), 105-122. doi:10.1583/1545-1550(2000)007<0105:FGAEAO>2.3.CO;2

55. Riepe, G., Loos, J., Imig, H., Schroder, A., Schneider, E., Petermann, J., et al. (1997). Long-term in vivo alterations of polyester vascular grafts in humans. *European Journal of Vascular and Endovascular Surgery : The Official Journal of the European Society for Vascular Surgery, 13*(6), 540-548.

56. Chakfé, N., Dieval, F., Riepe, G., Mathieu, D., Zbali, I., Thaveau, F., et al. (2004). Influence of the textile structure on the degradation of explanted aortic endoprostheses. *European Journal of Vascular and Endovascular Surgery, 27*(1), 33-41. doi:10.1016/S1078-5884(03)00341-1

57. *Atrium interventional surgery: Advanta V12 covered stent* Retrieved 3/24/2013, 2013, from http://www.atriummed.com/EN/interventional/v12.asp

58. Allard, L., Soulez, G., Chayer, B., Qin, Z., & Cloutier, G. (2012). *Vascular imaging phantom of an abdominal aorta aneurysm with a visible thrombus.* Unpublished manuscript.

59. *Baylis medical canada - radiofrequency guidewire - PowerWire™ radiofrequency guidewire* Retrieved 3/24/2013, 2013, from http://www.baylismedicalcanada.com/pages/radio/powerwire.html

60. *Assessing radial tests for endovascular implants | MDDI medical device and diagnostic industry news products and suppliers* Retrieved 3/24/2013, 2013, from http://www.mddionline.com/article/assessing-radial-tests-endovascular-implants

61. D 3787 - 07: Standard test method for bursting strength of textiles - constant-rate-of-traverse (CRT) ball burst test. In: S. J. Bailey, N. C. Baldini, editors. Annual book of ASTM standards. West Conshohocken, PA: ASTM International; 2008. p. 859-862.

62. ISO 7198:1998(E): Cardiovascular implants - tubular vascular prostheses. In: International Organization for Standards, editor. 1st ed.; 1998. p. 1-48.

63. *Personal communications with Dr. Martin King* (2013). In Ruthrauff A. (Ed.)

APPENDICES

Appendix A: Radial Stiffness

An additional test was performed to demonstrate the cyclic hardening of the metal stents after 40 million cycles on the pulsatile fatigue tester, compared with un-fatigued controls. As there was no standard test method to use while keeping the devices intact, a new method was developed based on the loop strap method for nitinol stents described by Melissa Lachowitzer [60] and modified to fit this situation, a ½" twill weave cotton ribbon was given a short vertical cut (see Figure 47), and one of the ends was threaded through this opening to create a loop. Each end of the loop was attached to the pneumatic clamps of an Instron 5544 tensile tester (See Figure 48). The stent graft was inserted horizontally into the loop, which would then be tightened until it was closely holding the stent graft. The top end of the ribbon was then raised by the tester to 25% of the diameter of the stent graft at a rate of 100 mm/min.

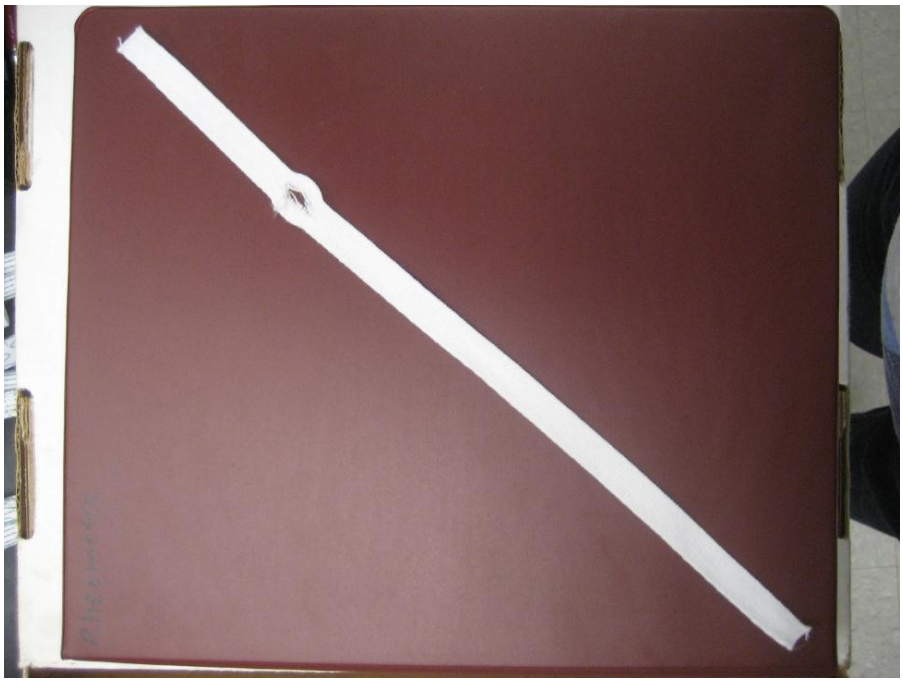

Figure 47: The loop strap used for the radial compression test shown flat.

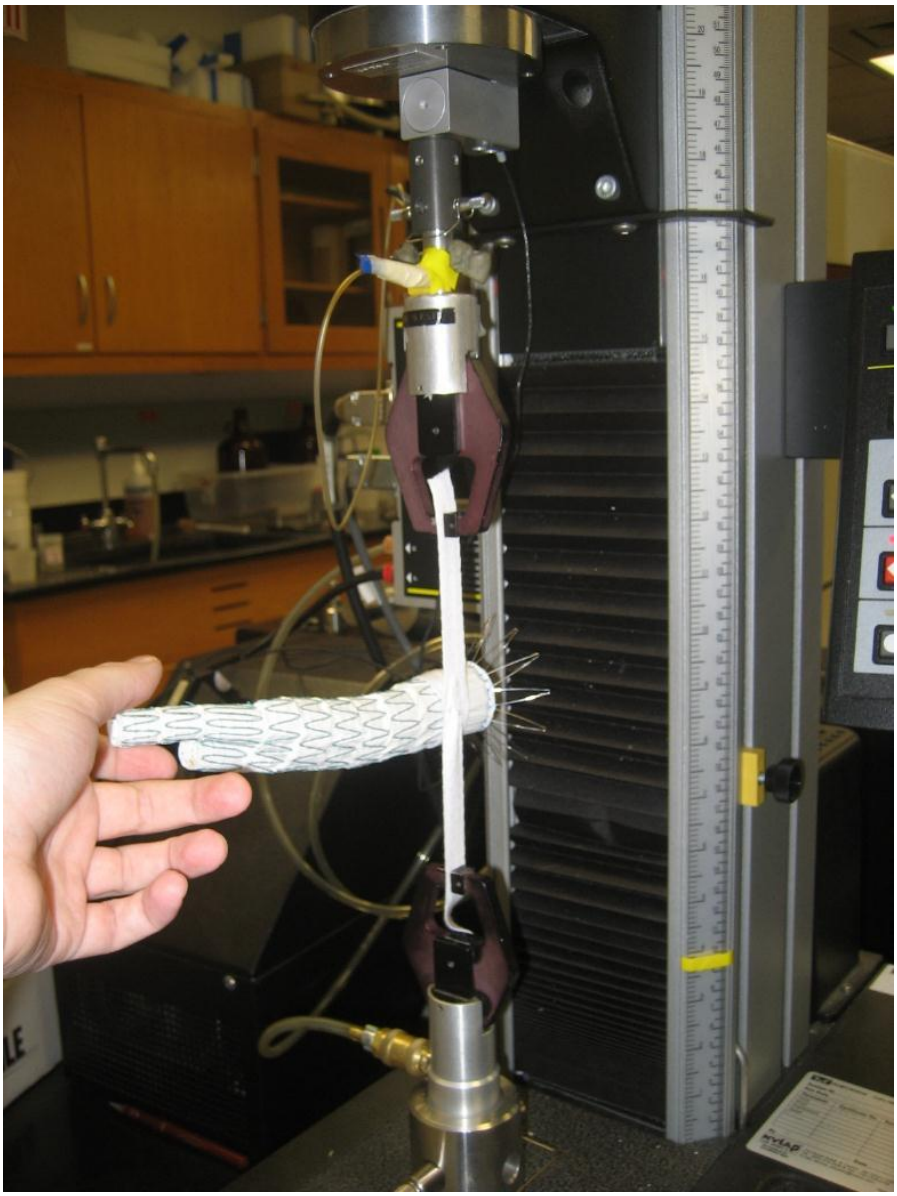

Figure 48: The loop strap and a sample loaded onto the Instron Tester for the Radial Compression Test. The end is being held up just to help balance it for the photo. It was not held up during the test.

Two positions were tested on each of the four devices; the loop strap placed over both fenestrations, and with the loop strap placed over a stent that didn't have a fenestration near it. The two control devices were only tested in one position, over a stent. Since each fenestration

was in a unique position, the other position would give a proper comparison. Each position was tested five times in order to get an average force. Prior to beginning this test, the iliac limbs were removed by gently compressing and pulling on them. This was done to reduce the weight of the distal end of the devices and create a more even balance when placed horizontally.

The idea behind this test is that the section of the stent graft intended to be tested would be inserted into the loop, and the loop reduced in size until the graft was compressed to 75% of its diameter. The maximum force required to do this would be measured. As the ribbon itself has a small amount of stretch, the values recorded were taken only as relative measurements to be compared amongst samples. A statistical analysis was performed on these measurements.

Statistical Analysis

As there were only four samples in total, this study was designed to be a demonstration study rather than provide statistical data. However, the data from the radial stiffness test was able to be analyzed due to the number of measurements taken for each location on each sample. A single factor ANOVA test was performed on all of the samples with a 95% confidence interval. Two following ANOVA tests were performed on only the Cook samples, and only the Medtronic samples, in order to properly compare them. In order to see which specific samples were statistically different from one another, line graphs with markers for each mean were plotted, the line remove, and standard error bars added. If two different error bars have some common values along the y-axis, then the measurements for the samples are not

statistically different. If they do not have any common values, then the measurements are statistically different. The Medtronic devices and Cook devices were only compared amongst themselves, as the stents in each type of graft was made of a different material.

Using the ANOVA test and chart method described above, it can be seen that the average force required to compress the stent grafts by 25% of their original diameter at each location is larger than the force required for the control graft. This demonstrates the cyclic 'hardening' of the stainless steel stents due to pulsatile fatigue. The measurements for both cook devices can be seen in Appendix B, and the ANOVA based graph can be seen in Figure 48.

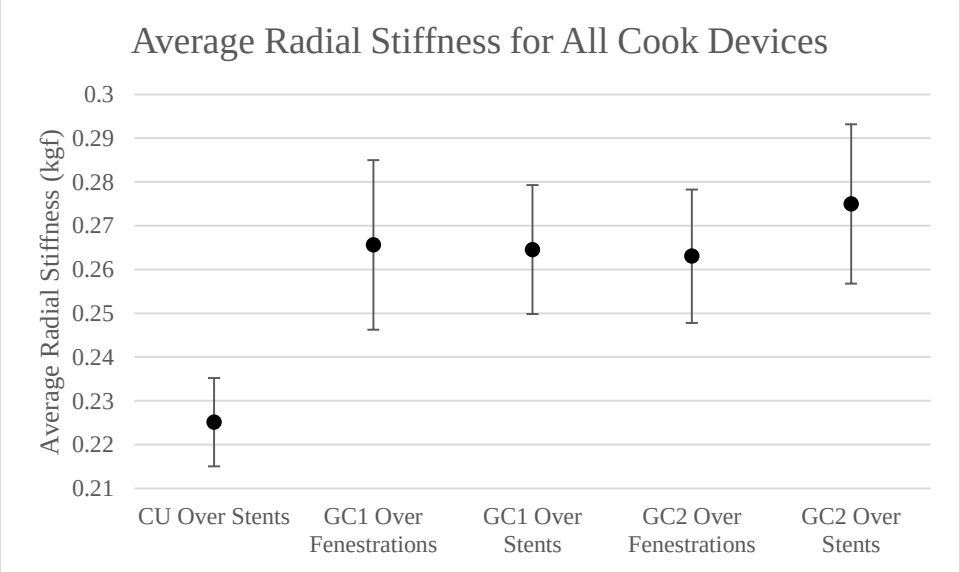

Figure 49: The Average Radial Stiffness of the Cook devices with Standard Error Bars

Using the same technique described as above, the Medtronic control, GM1, and GM2 devices were checked for statistical differences in their radial stiffness at different locations. The Medtronic devices were not as consistent as the Cook devices. The measurements taken show that there was no cyclic hardening in the nitinol, but a weakening instead due to the pulsatile fatigue.

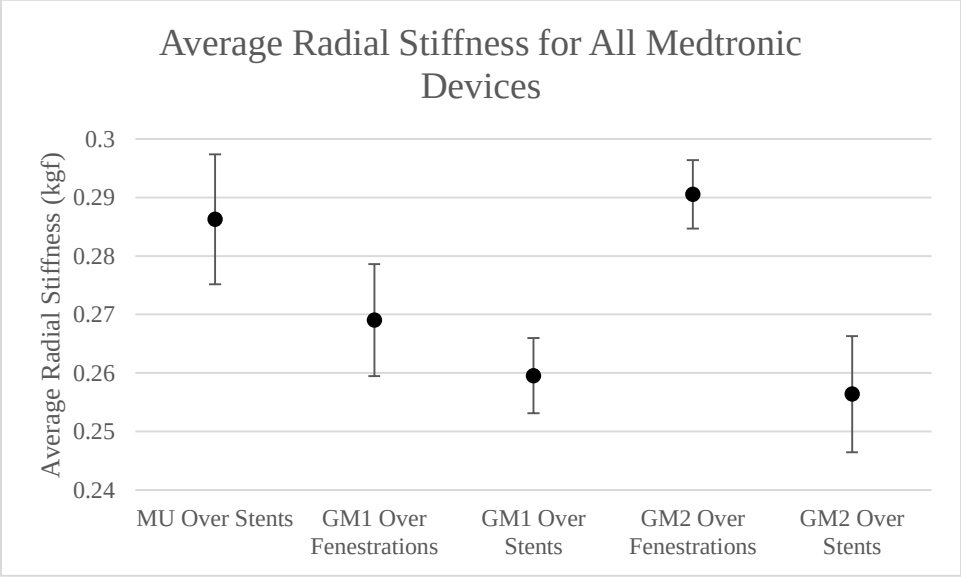

*Figure 50: The Average Radial Stiffness for Medtronic Devices with Standard Error (1.96*StdErr) Bars*

Appendix B: ANOVA Tests and Additional Tables

Anova: Single Factor

SUMMARY

Groups	*Count*	*Sum*	*Average*	*Variance*	*1.96*StdErr*
CU Over Stents	5	1.1257	0.22514	0.000133	0.010093486
GC1 Over Fenestrations	5	1.32807	0.265614	0.000488	0.019355691
GC1 Over Stents	5	1.32267	0.264534	0.000282	0.014714777
GC2 Over Fenestrations	5	1.31521	0.263042	0.000302	0.015241243
GC2 Over Stents	5	1.37481	0.274962	0.00043	0.018185634

ANOVA

Source of Variation	*SS*	*df*	*MS*	*F*	*P-value*	*F crit*
Between Groups	0.007457	4	0.001864	5.701763	0.003136206	2.866081
Within Groups	0.006539	20	0.000327			
Total	0.013996	24				

Single-Factor ANOVA analysis for the radial stiffness measurements of the Cook devices, plus a column for the standard error.

Anova: Single Factor

SUMMARY

Groups	*Count*	*Sum*	*Average*	*Variance*	*1.96*StdErr*
MU Over Stents	5	1.4313	0.28626	0.00016	0.011088858
GM1 Over Fenestrations	5	1.34526	0.269052	0.000119	0.009566608
GM1 Over Stents	5	1.2977	0.25954	5.4E-05	0.006443585
GM2 Over Fenestrations	5	1.45257	0.290514	4.46E-05	0.005851191
GM2 Over Stents	5	1.28188	0.256376	0.000128	0.009933663

ANOVA

Source of Variation	*SS*	*df*	*MS*	*F*	*P-value*	*F crit*
Between Groups	0.004768	4	0.001192	11.77373	4.44153E-05	2.866081
Within Groups	0.002025	20	0.000101			
Total	0.006793	24				

Single-Factor ANOVA Analysis of the radial stiffness measurements for the Medtronic Devices, plus a column for the standard error.

Specimen	Force1 (kgf)	Force2 (kgf)	Force3 (kgf)	Force4 (kgf)	Force5 (kgf)	Avg (kgf)	Std Dev (kgf)
CU Over Stents	0.240	0.230	0.213	0.228	0.214	0.225	0.012
GC1 Over Fenestrations	0.292	0.280	0.244	0.270	0.242	0.266	0.022
GC1 Over Stents	0.286	0.275	0.266	0.249	0.246	0.265	0.017
GC2 Over Fenestrations	0.277	0.257	0.251	0.285	0.245	0.263	0.017
GC2 Over Stents	0.295	0.260	0.277	0.248	0.295	0.275	0.021
MU Over Stents	0.301	0.295	0.289	0.270	0.277	0.286	0.013
GM1 Over Fenestrations	0.275	0.272	0.275	0.250	0.274	0.269	0.011
GM1 Over Stents	0.271	0.258	0.253	0.254	0.261	0.260	0.007
GM2 Over Fenestrations	0.295	0.293	0.297	0.287	0.281	0.291	0.007
GM2 Over Stents	0.272	0.259	0.260	0.245	0.245	0.256	0.011

Appendix Table 1: The Radial Stiffness Measurements for all of the devices.